Clays and Clay Minerals, Vol. 57, No. 1, 1–24, 2009.

SIGNIFICANCE OF PHYLLOSILICATE MINERALOGY AND MINERAL CHEMISTRY IN AN EPITHERMAL ENVIRONMENT. INSIGHTS FROM THE PALAI-ISLICA Au-Cu DEPOSIT (ALMERÍA, SE SPAIN)

JAVIER CARRILLO-ROSÚA[1,*], SALVADOR MORALES-RUANO[2,3], IÑAKI ESTEBAN-ARISPE[2], AND PURIFICACIÓN FENOLL HACH-ALÍ[2,3]

[1] Departamento de Didáctica de las Ciencias Experimentales, Universidad de Granada, Facultad de Ciencias de la Educación, Campus de Cartuja, 18071, Granada, Spain

[2] Departamento de Mineralogía y Petrología, Universidad de Granada, Facultad de Ciencias, Avd. Fuentenueva s.n., 18002, Granada, Spain

[3] Instituto Andaluz de Ciencias de la Tierra, CSIC Universidad de Granada, Facultad de Ciencias, Avd. Fuentenueva s.n., 18002, Granada, Spain

Abstract—Phyllosilicate mineralogy is key to understanding hydrothermal processes within accepted epithermal deposit models but little information has been published about the mineral chemistry of epithermal deposits. X-ray diffraction, optical and electronic microscopy (scanning and transmitted), electron microprobe, and Fourier transform infrared spectroscopy were used in this work to study phyllosilicates in the Palai-Islica Au-Cu epithermal, volcanic-hosted deposit, in order to link phyllosilicate mineralogy and mineral chemistry to ore genesis. Different phyllosilicate assemblages are characteristic of two types of mineralization, and related hydrothermal alteration. Chlorite and mica appear in polymetallic quartz veins with sulfides, and in the related chloritic and sericitic hydrothermal alteration. These minerals have notable textural and chemical differences (*i.e.* Fe/(Fe+Mg), Si and Al in chlorite and illitic and phengitic components in mica) amongst veins and altered rocks, revealing different genetic conditions. These chemical features also distinguish propylitic and regional, non ore-related, low-temperature alteration. Hot hydrothermal fluids of near-neutral pH are responsible for vein mineralization and alteration. Illite, interstratified illite-smectite, kaolinite, and pyrophyllite are characteristic, with a distribution pattern by zones, of the intermediate argillic and advanced argillic alteration around areas of silicification. In the latter, native gold appears associated with interstratified illite-smectite, suggesting a relatively low-temperature formation. Hot, low-pH fluids are responsible for this mineralization and alteration assemblage. The present study contributes to epithermal models showing the co-existence of two different alteration styles in the same hydrothermal system.

Key Words—Chlorite, Epithermal, Gold, Mica, Spain, Intermediate-sulfidation, Volcanic-hosted.

INTRODUCTION

Hydrothermal ore deposits containing gold, silver, and different base metals have been extracted in the Cabo de Gata-Cartagena volcanic belt, in southeastern Spain, since 2000 BC. More than 3000 mining sites have been identified in the area and in the last century the region became one of the most important base-metal producers in Europe. In recent years, the area has been targeted by mineral exploration companies looking for gold and copper (Rodalquilar and Herrerias since 1992; Arribas *et al*., 1995; Carrillo-Rosúa *et al*., 2003c). These hydrothermal deposits range from epithermal to mesothermal, and vary enormously in terms of their host rocks (rhyolites to andesites, schists, or sedimentary rocks), ore mineral textures, associations, paragenetic sequences, and proportions of precious metals (*e.g.* Morales-Ruano, 1994; Arribas and Tosdal, 1994; Arribas *et al*., 1995; Morales-Ruano *et al*., 2000). Bentonite-type clay deposits are also found in the area (formed at low temperature, <100ºC, Leone *et al*., 1983; Caballero *et al*., 1985, 2005) and extracted for industrial purposes.

Therefore, a great variety of phyllosilicates and alteration assemblages might be expected in the Cabo de Gata–Cartagena volcanic belt and these are interesting for two reasons: firstly as an indicator of potential metalliferous deposits, and secondly as an industrial resource in their own right. Detailed mineralogical studies of phyllosilicates have been performed in the bentonitic, low-temperature assemblage deposits (*e.g.* Caballero *et al*., 2005, and references therein), whereas studies of the high-temperature group of deposits have been more preliminary in nature (Arribas *et al*., 1995; Morales-Ruano *et al*., 2000).

The present research focuses on the Palai-Islica deposit, where recent exploration activity has demonstrated the presence of Au-Cu mineralization, related to the outcropping of an area of pervasive hydrothermal alteration (Morales-Ruano *et al*., 2000). A study using X-ray diffraction (XRD), optical microscopy, scanning electron microscopy (SEM), electron microprobe analy-

* E-mail address of corresponding author:
fjcarril@ugr.es
DOI: 10.1346/CCMN.2009.0570101

sis (EMPA), transmission electron microscopy (TEM), and Fourier transform infrared (FTIR) spectroscopy was performed. The main object of the research was to characterize the mineralogy and mineral chemistry of phyllosilicates related to the ore mineralization, and to discuss hydrothermal alteration typology and its implication in ore genesis. This argument falls within the classification and discussion of epithermal deposits (*e.g.* Simmons *et al*., 2005). The Simmons work is noteworthy because it shows the co-existence of two different alteration styles in the same hydrothermal system. Special mention should also be made of the mineralogical transformation from volcanic rocks to phyllosilicates during hydrothermal activity, as well as the chemistry of phyllosilicates and their relationship to the conditions of the hydrothermal fluids.

GEOLOGICAL BACKGROUND

The Palai-Islica is a Au-Cu epithermal deposit hosted by calc-alkaline rocks of the Cabo de Gata–Cartagena volcanic belt (Figure 1a), which comprises part of the eastern end of the Internal Zone of the Betic Cordillera. This Neogene volcanic belt, with different series of volcanic rocks (*i.e.* calc-alkaline, shoshonitic, potassic calc-alkaline, ultrapotassic, and basaltic series, López Ruiz and Rodriguez Badiola, 1980), formed within the context of compression, followed by an extensional event (Dewey, 1988; García Dueñas *et al*., 1992) and strike-slip movements in which volcanism occurs (*e.g.* Hernandez *et al*., 1987; Fernández Soler, 1996; Turner *et al*., 1999). Associated with this magmatism, hydrothermal systems developed, controlled by fault and fracture systems. The hot fluids (up to 400−450ºC, Morales Ruano, 1994) reacted strongly with the host rocks and, in some districts mainly located within the calc-alkaline zone, gave rise to broad areas of alteration hosting metallic mineralization: Cabo de Gata (Pineda Velasco, 1984), Rodalquilar (*e.g.* Arribas *et al*., 1995), and Palai-Islica (Morales-Ruano *et al*., 2000; Carrillo-Rosúa *et al*., 2003a). Palai-Islica (~4 km^2) is one of these alteration areas (Figure 1b), now a target of mineral exploration companies for gold and copper (Morales-Ruano *et al*., 2000), near the town of Carboneras (Almería province, SE Spain), over an extensive zone of breccias and auto-breccias of andesites/dacites which are ~10 Ma old (Bellon *et al*., 1983; Fernandez Soler, 1996). These rocks (Fernández Soler, 1996), which have a very porphyritic texture, are made up of phenocrysts of bytownite and hornblende (up to 1 cm wide) ± clinopyroxene and orthopyroxene. Quartz, Fe-Ti oxides, apatite, and zircon occur in accessory amounts.

SAMPLES AND METHODOLOGY

Samples were obtained from the mineralized area and from hydrothermally altered volcanic rocks at Palai-Islica. Two hundred and sixty-two samples selected from 21 drill cores and from a surface-sampling campaign were studied. Whole-rock powders, oriented aggregates of <2 μm fractions (with ethylene glycol and dimethyl sulfoxide solvation and without treatment), thin sections, a selection of ion-milled specimens, and suspension of these samples over Cu grids were prepared to determine the mineralogical, chemical, and textural characteristics of phyllosilicates in this deposit. The analytical equipment used included transmitted light microscopy and XRD (Philips PW 1710, with CuKα radiation, graphite monochromator, and automatic divergence slit) at the Department of Mineralogy and Petrology of the University of Granada, SEM (Zeiss DSM 950 and FESEM Leo Gemini 1530, with an EDX detector), EMPA (Cameca SX50, with WDX detector), and TEM (Philips CM20, with an EDAX solid-state EDX detector) at the Centro de Instrumentación Científica (CIC) of the University of Granada.

A total of 461 microanalyses of phyllosilicates were obtained using the different techniques (368 EMPA, 76 SEM, and 18 TEM). Natural and synthetic-certified standards were used to calibrate the EMPA, SEM, and TEM-AEM (analytical electron microscopy) quantitative analyses. The operating conditions were: 20 kV (EMPA and SEM) and 200 kV (TEM) accelerating potential, 30 nA (EMPA) and 1−2 nA (SEM) beam current, and acquisition times of 40−100 s (for X-ray peak and background for EMPA) and 100 s (SEM, TEM). Shorter counting times were used for K and Na in TEM-AEM analyses (30 s) and EMPA (20 s at peak and 20 s at background) to minimize alkali loss (Nieto *et al*., 1996). The AEM analyses were performed using a raster of 1000 Å × 200 Å in scanning mode for ion-milled samples and an analytical window of 1 μm × 1 μm in scanning transmission mode for powders dispersed over holey C-coated formvar Cu grids. The EMPA X-ray intensities acquired were corrected for atomic number, mass-absorption, and secondary fluorescence effects using the CAMECA-PAP version of the Pouchou and Pichoir (1984) procedure. The transformation of intensity ratios to concentration ratios in AEM analysis was made following the procedure of Cliff and Lorimer (1975). The structural formulae of mica and chlorite were calculated on the basis of 22 and 28 negative charges, $O_{10}(OH)_2$ and $O_{10}(OH)_8$, respectively.

Four samples of kaolinite (prepared as standard KBr pellets) were also analyzed by FTIR spectroscopy using a Nicolet 20SXB device (at the CIC at the University of Granada), in order to discriminate between kaolinite polytypes.

PREVIOUS DATA ON THE MINERALIZATION

Two different types of mineralization, quartz veins and veinlets with sulfides and dissemination in the silicification area, are recognized in the Palai-Islica deposit (Figure 2, Carrillo-Rosúa *et al*., 2003a).

https://doi.org/10.1346/CCMN.2009.0570101 Published online by Cambridge University Press

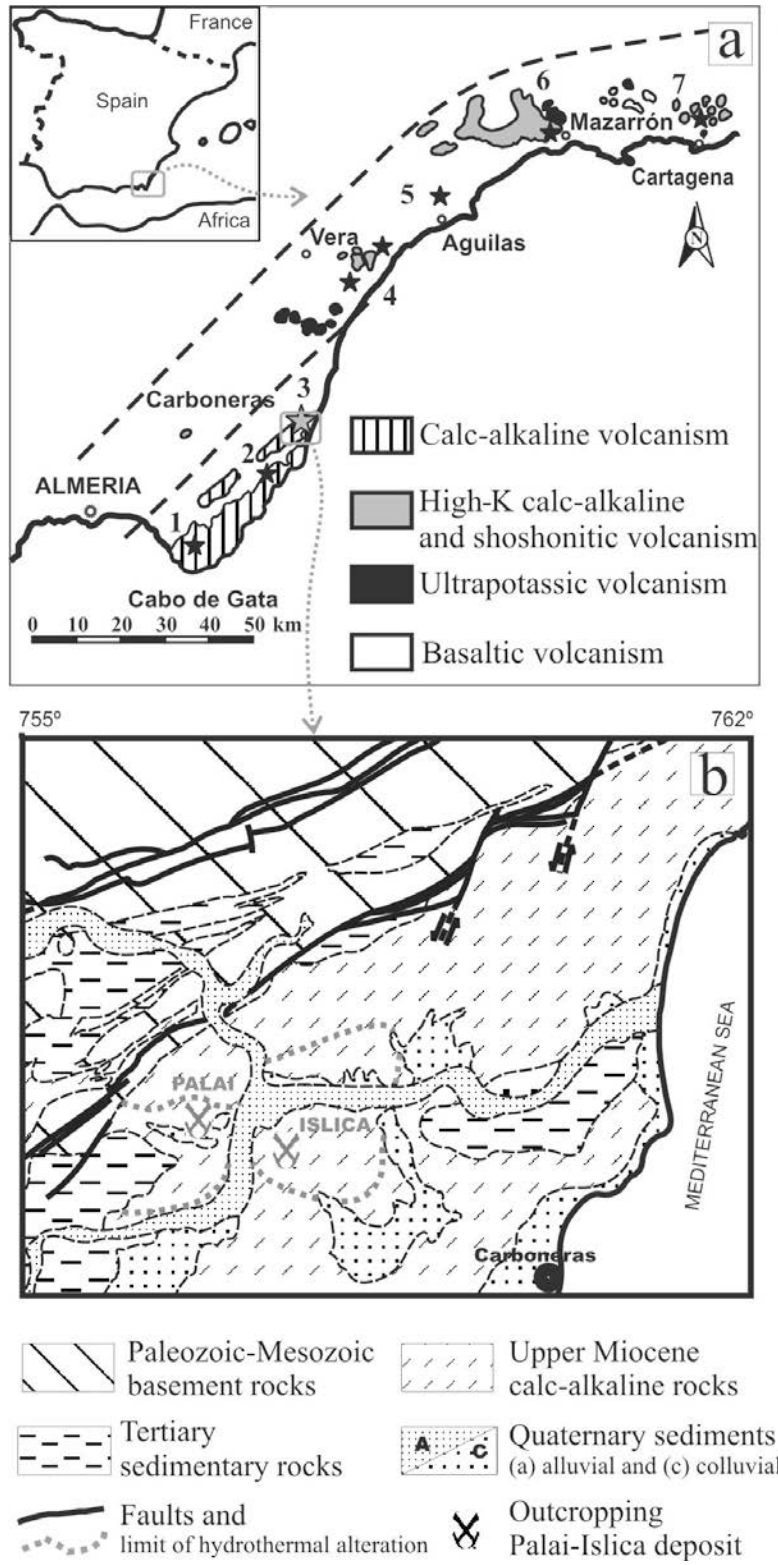

Figure 1. (a) Cabo de Gata–Cartagena volcanic province in SE Spain and the locations of the most important ore deposits in the volcanic belt (adapted from Lopez-Ruiz and Rodriguez-Badiola, 1980): (1) Cabo de Gata; (2) Rodalquilar; (3) Carboneras (Palai-Islica); (4) Herrerías and Sierra Almagrera; (5) Aguilas; (6) Mazarrón; (7) Cartagena. (b) Schematic geological map showing the location of the Palai-Islica deposit and the main geological units (adapted from IGME, 1974).

https://doi.org/10.1346/CCMN.2009.0570101 Published online by Cambridge University Press

Andesites/dacites, associated with this mineralization, show an important hydrothermal alteration, which is different in relation to the two types of mineralization.

(1) Veins and veinlets of quartz with sulfides

These comprise the majority of ore of the deposit, located between +70 and −90 m above sea level (m.a.s.l.). These veins, sometimes stockwork-like and very penetrative, are very rich in sulfides. Although the veins have a sub-vertical trend, two main sub-horizontal levels have been recognized with enrichment in Au, Ag, Zn, Pb, Cd, As, and Sb, with free gold grains and with fluid inclusions showing distinct characteristics (wide variation in salinity, 20−30 wt.% eq. NaCl, over a narrow temperature range of −200 to 250ºC) relative to the rest of the deposit (Morales-Ruano *et al*., 2000). The ore mineralogy consists of pyrite with occasionally large amounts of chalcopyrite, sphalerite, and galena. Accessory phases are very diverse: Au-Ag alloys and different Ag-bearing sulfides and sulfosalts being the most notable from an economic point of view (Carrillo-Rosúa *et al*., 2002, 2003a, 2003b, 2008a). The main gangue minerals are quartz, white mica ('sericite'), and chlorite with minor quantities of barite, gypsum, dolomite, and siderite (Carrillo-Rosúa *et al*., 2003a).

In relation to hydrothermal alteration, the andesites/dacites, which host the veins, are totally transformed to quartz, white mica plus chlorite, and, to a lesser extent, pyrite, dolomite, albite, and epidote (Carrillo-Rosúa *et al*., 2003a). Hydrothermal alteration is pervasive and the only minerals which remain are quartz, zircon, and apatite, though apatite undergoes chemical transformation (Carrillo-Rosúa *et al*., 2005). White mica and chlorite (±pyrite, albite, and epidote) are the minerals which characterize the proximal hydrothermal alteration zone. In distal areas, at the edges of the deposit, major phenocrysts remain unaltered: namely plagioclase, and in the less altered zones, hornblende and pyroxene. The

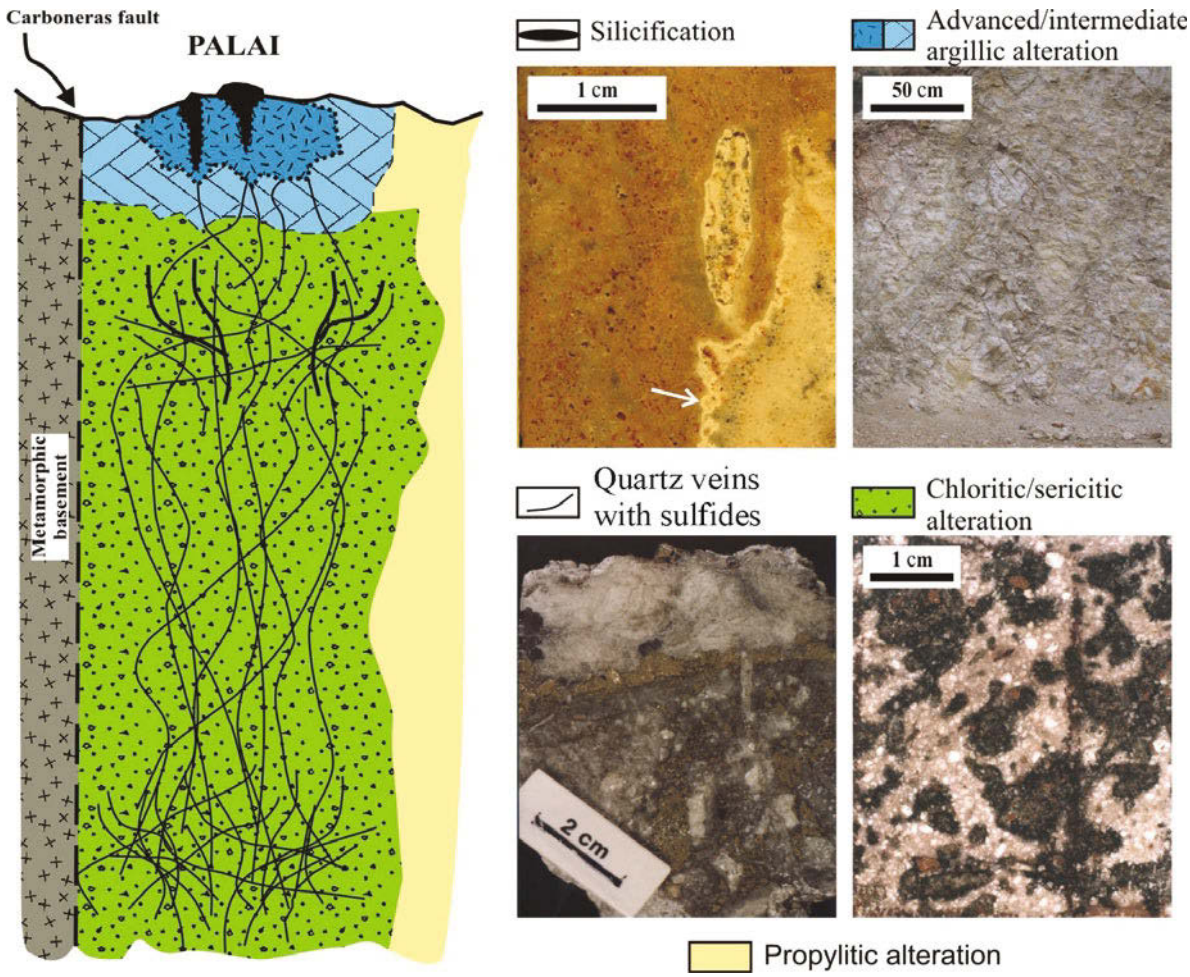

Figure 2. Schematic of the Palai-Islica deposit, including the different kinds of mineralization. In the silicification, an arrow indicates a phyllosilicate micro-vein. (A high-quality color version of this figure is available from www.clays.org/journal/JournalDeposits.html)

https://doi.org/10.1346/CCMN.2009.0570101 Published online by Cambridge University Press

Table 1. Summary of the distribution of phyllosilicates at the Palai-Islica deposit, in relation to the primary mineralogy of the host rock.

	Veins	Sericitic alteration	Chloritic alteration	Silicification	Advanced argillic alteration	Intermediate argillic alteration
Chlorite	XX	X (mafic phenocrysts)	XXX (matrix and mafic phenocrysts)			
Mica	XX	XXX (matrix, plagioclase and mafic phenocrysts)	X (matrix and plagioclase)		XX	XX
Interstratified illite-smectite				X	X	X
Kaolinite					XX	
Pyrophyllite					XX	

X: scarce; XX: abundant; XXX: very abundant

alteration at the edges of the deposit could be defined as propylitic, with chlorite, epidote, and calcite/dolomite.

(2) Dissemination in the silicification area

This consists of complete replacement of the volcanic rock by quartz. Sometimes it is very porous, with holes corresponding to old volcanic phenocrysts, like vuggy silica textures and is found at the surface of the deposit between +70 and +100 m.a.s.l. Ore minerals, mainly disseminated in holes, are very scarce, with the mineralogy consisting mainly of pyrite, with minor Cu sulfides and native gold and copper (Carrillo-Rosúa *et al*., 2002). Apart from the typical coarse-grained quartz, the gangue minerals include microcrystalline quartz, white mica, and barite, gypsum, jarosite, natrojarosite, and natroalunite in later veins.

The silicification area has halos of advanced argillic and intermediate argillic alteration characterized by quartz, pyrophyllite, kaolinite, illite, and interstratified illite-smectite. In distal zones, propylitic alteration is also evident.

MINERALOGICAL, TEXTURAL, AND CHEMICAL CHARACTERISTICS OF THE PHYLLOSILICATES

The mineralogical differences, especially in the phyllosilicates, between the two types of mineralization in the Palai-Islica deposit (Table 1) are noteworthy. The main mineralogical, textural, and chemical characteristics of the phyllosilicates in relation to the mineralization types and the related, hydrothermally altered, host rock are described.

Quartz veins with sulfides and related hydrothermal alteration

Optical microscopic observations and XRD study of the veins and related hydrothermal alteration areas revealed that phyllosilicates are very abundant, but only chlorite and white mica have been recognized.

Chlorite textures. Chlorite appears as spherulitic aggregates (~100 μm) and rarely as inclusions in pyrite grains in the quartz veins (Figure 3a). The spherulitic aggregates show lighter rims in respect to cores in backscattered images (Figure 3b).

Chlorite also appears, replacing amphibole, pyroxene, and the groundmass in the hydrothermal alteration area. Chlorite replacing mafic phenocrysts often develops larger crystals than the groundmass and is oriented. Thus, the basal plane of chlorite is parallel to the *b* and *c* axes of hornblende and pyroxene or, in other words, the (001) plane of chlorite is parallel to the (010) planes of the amphibole and pyroxene (Figure 3c,d). Occasionally, the mafic phenocrysts transformed to chlorite appear as xenocrysts within the quartz veins (Figure 3e). Chlorite very rarely replaces plagioclase, generally being fine-grained as in the groundmass and, in some cases, in mafic phenocrysts.

In the external zone characterized by propylitic alteration, or even far from the deposit in zones of regional alteration, due to widespread meteoric alteration, chlorite is also found replacing mafic phenocrysts, but generally fine-grained disappearing oriented textures through the outside of the veins (Figure 3f). Studies by TEM of this chlorite show intercalations of 10 Å K-rich layers.

Chlorite mineral chemistry. Table 2 and Figure 4 summarize the microanalyses of chlorite. Fe/(Fe+Mg) is directly proportional to Al_{total} or ^{IV}Al and Mn, and inversely proportional to Si (Figure 4a–c). Si is inversely proportional to Al_{total} (Figure 4d). For the whole data set, the number of interlayer cations (K+Na+2Ca) is proportional to the number of octahedral vacancies, although with a greater slope for chlorite from the propylitic alteration than for chlorite from the hydrothermal alteration area related to veins (Figure 4e).

Pronounced chemical differences are observed in terms of the Si, Al, Fe, Mg, and Mn contents of chlorite

https://doi.org/10.1346/CCMN.2009.0570101 Published online by Cambridge University Press

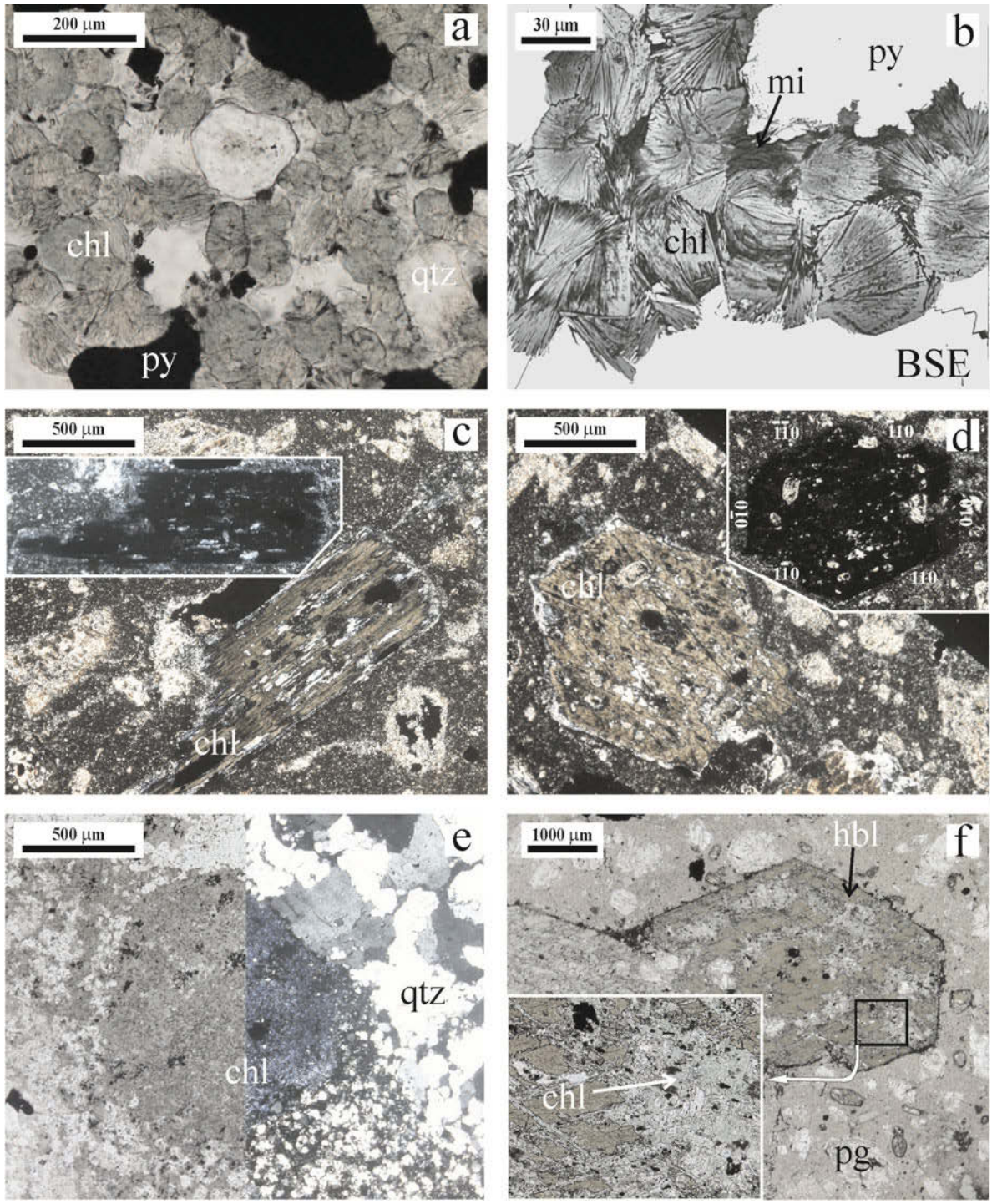

Figure 3. Transmitted light (plane-polarized and crossed-polarized light) and backscattered electron (BSE) photomicrograph of chlorites. (a,b) Spherulitic aggregates of chlorite (chl) intergrowing with coarse quartz (qtz) and sulfides (py: pyrite) in the veins. In the BSE image (b) dark cores and bright rims in chlorite are observed; also interstitial mica (mi) possibly replacing chlorite. (c,d) Prismatic, basal section of hornblende (in positions of maximum of illumination and extinction) replaced by coherent, oriented chlorite in the hydrothermal alteration related to quartz veins. (e) Chlorite precedent of hornblende replacement within a quartz vein. (f) Incipient replacement of hornblende (hbl) by chlorite (chl) in the propylitic alteration. (A high-quality color version of this figure is available from www.clays.org/journal/JournalDeposits.html)

https://doi.org/10.1346/CCMN.2009.0570101 Published online by Cambridge University Press

Table 2. EMPA analyses of chlorite in the quartz veins and the related hydrothermal alteration of the Palai-Islica deposit (normalized to $O_{10}(OH)_8$).

	— Veins (n = 43) —				– Alteration (n = 67) –				– Transitional (n = 36) –				– Propylitic (n = 41) –			
Wt.%	Min	Max	Ave	S.D.	Min	Max	Ave	S.D.	Min	Max	Ave	S.D.	Min	Max	Ave	S.D.
SiO_2	20.05	26.84	24.60	1.20	26.73	33.48	30.35	1.19	23.94	28.87	27.22	1.23	29.18	34.99	31.45	1.50
TiO_2	0.01	0.06	0.03	0.01	0.00	0.54	0.03	0.07	0.00	0.07	0.02	0.01	0.00	23.00	4.34	8.20
Al_2O_3	13.91	21.65	19.53	1.73	16.41	20.55	18.43	1.02	16.20	20.94	19.30	1.17	0.00	21.13	13.98	7.52
FeO	24.67	35.83	30.94	2.82	2.68	21.73	14.71	4.39	18.97	27.30	22.50	2.40	12.38	22.17	17.53	2.46
MgO	5.71	11.68	8.81	1.84	18.32	30.77	22.36	2.85	11.38	18.09	15.09	1.90	13.82	20.53	18.12	1.31
MnO	0.22	1.05	0.50	0.23	0.12	0.80	0.35	0.15	0.39	0.77	0.55	0.10	0.07	0.72	0.46	0.16
CaO	0.00	0.12	0.05	0.03	0.03	0.15	0.08	0.03	0.03	0.14	0.07	0.03	0.03	0.63	0.23	0.16
K_2O	0.00	0.26	0.05	0.05	0.00	0.47	0.07	0.09	0.01	0.16	0.07	0.04	0.03	2.34	0.48	0.46
Na_2O	0.00	0.09	0.04	0.03	0.00	0.09	0.03	0.02	0.00	0.08	0.03	0.02	0.01	0.39	0.08	0.07
a.p.f.u.																
Si	2.65	3.05	2.79	0.08	2.89	3.14	3.05	0.05	2.86	2.99	2.92	0.04	3.01	3.61	3.19	0.13
Ti	0.00	0.01	0.00	0.00	0.00	0.04	0.00	0.01	0.00	0.01	0.00	0.00	0.00	0.00	0.00	0.00
^{IV}Al	0.95	1.35	1.21	0.08	0.86	1.11	0.95	0.05	1.01	1.14	1.08	0.04	0.39	0.99	0.81	0.13
^{VI}Al	1.15	1.52	1.40	0.07	1.09	1.41	1.23	0.08	1.23	1.50	1.36	0.07	1.06	2.03	1.38	0.19
Fe	2.41	3.40	2.94	0.27	0.21	1.86	1.24	0.38	1.70	2.43	2.02	0.23	1.02	1.92	1.49	0.22
Mg	0.98	1.91	1.49	0.28	2.79	4.26	3.34	0.34	2.10	2.80	2.41	0.22	2.03	3.07	2.74	0.20
Mn	0.02	0.10	0.05	0.02	0.01	0.07	0.03	0.01	0.04	0.07	0.05	0.01	0.01	0.06	0.04	0.01
Vac.	0.04	0.25	0.12	0.04	0.07	0.29	0.16	0.05	0.09	0.24	0.16	0.04	0.09	0.87	0.35	0.17
Ca	0.00	0.01	0.01	0.00	0.00	0.01	0.01	0.00	0.00	0.02	0.01	0.00	0.00	0.07	0.03	0.02
K	0.00	0.04	0.01	0.01	0.00	0.06	0.01	0.01	0.00	0.02	0.01	0.01	0.00	0.29	0.06	0.06
Na	0.00	0.02	0.01	0.01	0.00	0.02	0.01	0.00	0.00	0.02	0.01	0.00	0.00	0.08	0.02	0.01
K+Na +2Ca	0.00	0.07	0.03	0.02	0.01	0.09	0.03	0.01	0.01	0.05	0.03	0.01	0.01	0.31	0.10	0.07

n: number of analyses; Min: minimum.; Max: maximum.; Ave: average; S.D.: standard deviation; Vac.: vacancies. Veins: chlorite from the quartz veins with sulfides; Alteration: chlorite from the hydrothermal alteration area related to quartz veins with sulfides; Transitional: chlorite from the quartz veins but which originated in the hydrothermal alteration area ('xenocrysts'). Propylitic: chlorite from the most marginal zones of the Palai-Islica deposit, in areas of propylitic/regional low-temperature alteration.

from the different textural types. Spherulitic aggregates of chlorite from the veins have the greatest Al_{total} contents (2.26–2.85 a.p.f.u.) and Fe/(Fe+Mg) ratio (0.56–0.78), small Si contents (2.65–3.05 a.p.f.u.), and variable Mn contents (0.02–0.10 a.p.f.u.). No clear relationships were observed between the different elements (Figure 4a–d). Chemical zonation, due to greater Fe/(Fe+Mg) ratios in the rims than in the cores, is revealed by backscattered images (Figure 3b). Chlorite in xenocrysts from the veins has a chemical composition which is between that of chlorite in spherulitic aggregates in the veins and that of chlorite in the hydrothermal alteration areas.

Chlorite in the hydrothermal alteration areas related to veins has large Si contents (2.89–3.14 a.p.f.u.), small Al_{total} contents (2.03–2.38 a.p.f.u.), and the smallest Fe/(Fe+Mg) ratio (0.05–0.40) of the chlorites analyzed (Table 2). The chemical tendencies are the same throughout, with the exception of Fe/(Fe+Mg) which is not related to ^{IV}Al (Figure 4a).

Chlorite in the propylitic hydrothermal alteration areas and in regional alteration areas has a distinctive composition characterized by intermediate and homogeneous Fe/(Fe+Mg) ratios (0.30–0.43) and the greatest Si contents (3.01–3.61 a.p.f.u.), the most interlayer-cations (0.01–0.32 a.p.f.u.), and the most octahedral vacancies (0.09–0.87 a.p.f.u.). Chlorite from the propylitic alteration area proper has intermediate Al (2.19–2.61 a.p.f.u.) and large Mn (0.04–0.06 a.p.f.u.) and K (average 0.08 a.p.f.u.) contents, while chlorite in less altered rocks (propylitic to regional alteration areas) has small Mn (0.01–0.05 a.p.f.u.) and Al_{total} (1.76–2.28 a.p.f.u.) and large Ca (average 0.03 a.p.f.u.) contents.

White-mica textures

White mica is the most abundant phyllosilicate. It appears in the veins as crystals and aggregates of crystals of variable size, from sub-microscopic to 100 μm. Mica appears disseminated, intergrown with quartz, interstitial to quartz or even as inclusions in quartz, and also as micro-veins (Figure 5a,b).

Mica is by far the most abundant phase replacing volcanic plagioclase (as phenocrysts or inclusions in amphibole and pyroxene). This mica varies from sub-microscopic to dozens of micrometers (typical 'sericite'), occasionally with the (001) mica packet parallel to faces of the plagioclase (Figure 5c,d) showing, in

https://doi.org/10.1346/CCMN.2009.0570101 Published online by Cambridge University Press

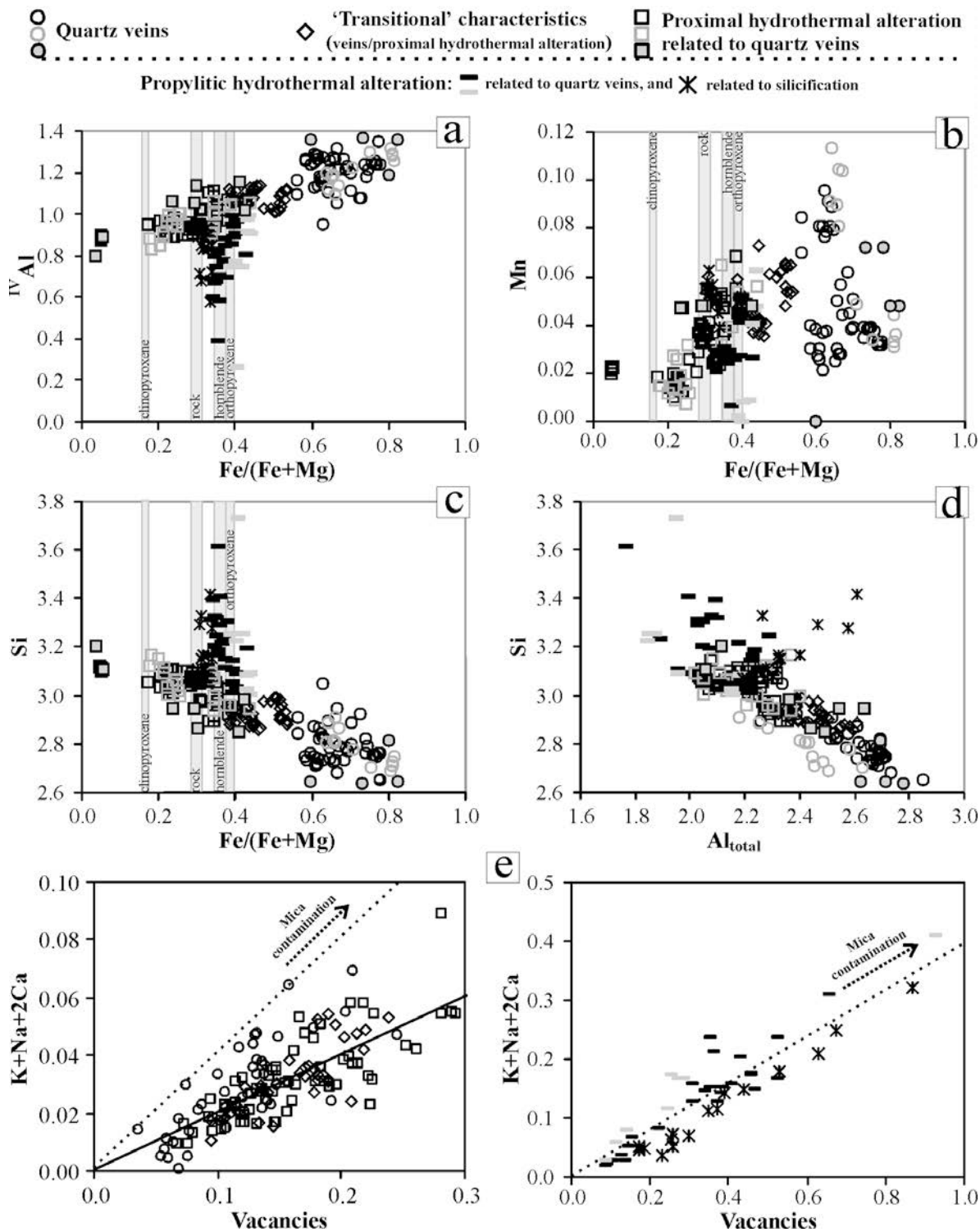

Figure 4. Binary diagrams showing compositional variations, expressed as atoms per formula unit (a.p.f.u.), between tetrahedral and octahedral cations and interlayer cations and vacancies in the different types of chlorites. Fe/(Fe+Mg) ratio data of the unaltered volcanic rock and phenocrysts (from Fernández Soler, 1996), which host the Palai-Islica deposit, are shown. EMPA analyses are plotted as open symbols, TEM-AEM analyses in gray-filled symbols, and SEM analyses as gray, open symbols. The influence of mica contamination and the correlation line in chlorite analyses are shown by dotted and solid lines, respectively (e).

https://doi.org/10.1346/CCMN.2009.0570101 Published online by Cambridge University Press

TEM images, a rare prismatic morphology (Figure 5e). Mica also replaces mafic phenocrysts as sub-microscopic or microscopic disoriented crystals (Figure 5f). Mica aggregates rarely have a 'palm' texture; coarse mica oriented in the mafic phenocrysts is more common (Figure 5g) in which case mica exclusively replaces the amphibole and pyroxene or it is accompanied by chlorite with the same orientation (Figure 5h). In cases where mica and chlorite coexist, 10 Å mica packets are found randomly interlayed in the chlorite stacks (Figure 5i). Mica also ranges from sub-microscopic to microscopic in the volcanic matrix, although fine-grained crystals are much more common.

The quartz veins are very penetrative. Thus, a wide range of transitional occurrences are observed between proper veins and hydrothermally altered volcanic rock. For instance, in the veins, mica often manifests characteristics of hydrothermal alteration: coarse-grained which arises from the transformation of ferromagnesian phenocrysts; and fine-grained which arises from the transformation of plagioclase (Figure 5j).

Finally, although mica polytypism has not been studied systemically, *tv* 1*M*, 2*M*, and 3*T* polytypes have been deduced by XRD and TEM, the first mainly in the hydrothermal alteration and the third only observed in the veins (Figure 6a,b).

White-mica mineral chemistry. Mica micro-analyses are summarized in Table 3 and in Figures 7 and 8. The number of interlayer cations (K+Na+2Ca) ranges between 0.65 and 0.82 a.p.f.u., with K the dominant cation, while the number of octahedral cations ranges between 1.99 and 2.15 a.p.f.u. The Fe/(Fe+Mg) ratio ranges between 0.08 and 0.82, although the majority of data range between 0.08 and 0.43. Al_{total} correlates inversely with Si ($m \approx 2$, Figure 7a), and the number of interlayer cations does not correlate with either Al_{total} or Si (Figure 7b,c). There is a negative correlation between Fe+Mg and Al_{total}, even better with ^{VI}Al (Figure 7d), and a roughly positive correlation between Fe+Mg and Si (Figure 7e). The Fe content is almost always less than the Mg content (Fe/(Fe+Mg)>0.5) (Figure 7f).

The micas from different locations show some differences in terms of chemical composition. The mica in the veins has relatively large Al (2.20–2.65 a.p.f.u.), K (0.60–0.82 a.p.f.u.), and F (0.00–0.08 a.p.f.u.) contents, while the Si content is small (3.23–3.44 a.p.f.u.) (Figures 7, 8). (Fe+Mg) is very variable, ranging up to relatively large values (0.08–0.43 a.p.f.u.). The analyses with large Fe+Mg values move away from the linear tendency of Fe+Mg *vs.* Al_{total} seen in the majority of analyses (Figure 7d). Micas in the veins but originally from the hydrothermal alteration areas show greater K and F contents than mica which originated directly from the veins (Figure 8).

Mica in the hydrothermal alteration area is characterized by relatively large Si and small K (0.60–0.77 a.p.f.u.) contents, by small numbers of interlayer cations (0.65–0.86 a.p.f.u.), and by small F (0.00–0.06 a.p.f.u.) contents. Relatively coarse-grained mica replacing plagioclase has small Si and Fe and larger Al and K contents than mica replacing ferromagnesian phenocrysts. Fine-grained mica which replaces plagioclase is relatively rich in Si, K, F, and Fe, and relatively poor in Al compared to the other types of mica in the hydrothermal alteration area (Figures 7, 8, Table 3).

Silicification and related hydrothermal alteration

Phyllosilicates in the silicification area are very scarce and correspond to interstratified illite-smectite. They appear as aggregates in micro-veins in which native gold crystals are also in evidence (Figure 9a). These micro-veins formed after the main quartz generation event, but before the formation of sulfates (barite → Fe-Al sulfates → gypsum). Very fine-grained phyllosilicates (kaolinite, pyrophyllite, discrete illite, and illite-smectite interstratified) + quartz are the most abundant phases in hydrothermal alteration that encloses silicification. Around silicification areas, hydrothermally altered rocks show mineral zonation (Figure 2). (1) Proximal area – this consists of quartz, pyrophyllite, kaolinite, discrete illite, and interstratified illite-smectite. Zones closer to the silicification area are more quartz- and pyrophyllite-rich, the latter mineral disappearing toward peripheral zones. Pyrophyllite has a tendency to replace plagioclase, while quartz is enriched in the matrix. Kaolinite corresponds to kaolinite (±nacrite and dickite?) polytypes according to XRD and IR spectra patterns. (2) Distal zone – this is characterized by quartz, illite, and interstratified illite-smectite.

The prominence of interstratified illite-smectite is deduced from XRD patterns (following application of ethylene-glycol solvation), with a high proportion of illite layers (~90% according to Reynolds, 1980).

Electron microscopy, mainly TEM, confirms that interstratified illite-smectite is the only phyllosilicate found in the silicification area. Backscattered images show changes in composition at the scale of several micrometers (Figure 9b). In low-magnification TEM images, stacks of tabular phyllosilicates up to several micrometers thick are observed. Lattice-fringe images show layers always 10 Å thick, and SAED patterns also show a 10 Å periodicity, in a semi-ordered pattern (Figure 10). This is consistent with the local ordered pattern in a major disorder sequence. Detailed observation of the lattice-fringe images shows termination of several or individual layers in wedges (Figure 10a,b). Splitting of 10 Å layers into two 5 Å layers, which, hundreds of micrometers along, fuse with neighboring split layers, is also observed (Figure 10b). This might be related to screw dislocations, affecting the interstratified illite-smectite.

Phyllosilicate mineral chemistry. A considerable proportion of microanalyses of phyllosilicates, except possibly

https://doi.org/10.1346/CCMN.2009.0570101 Published online by Cambridge University Press

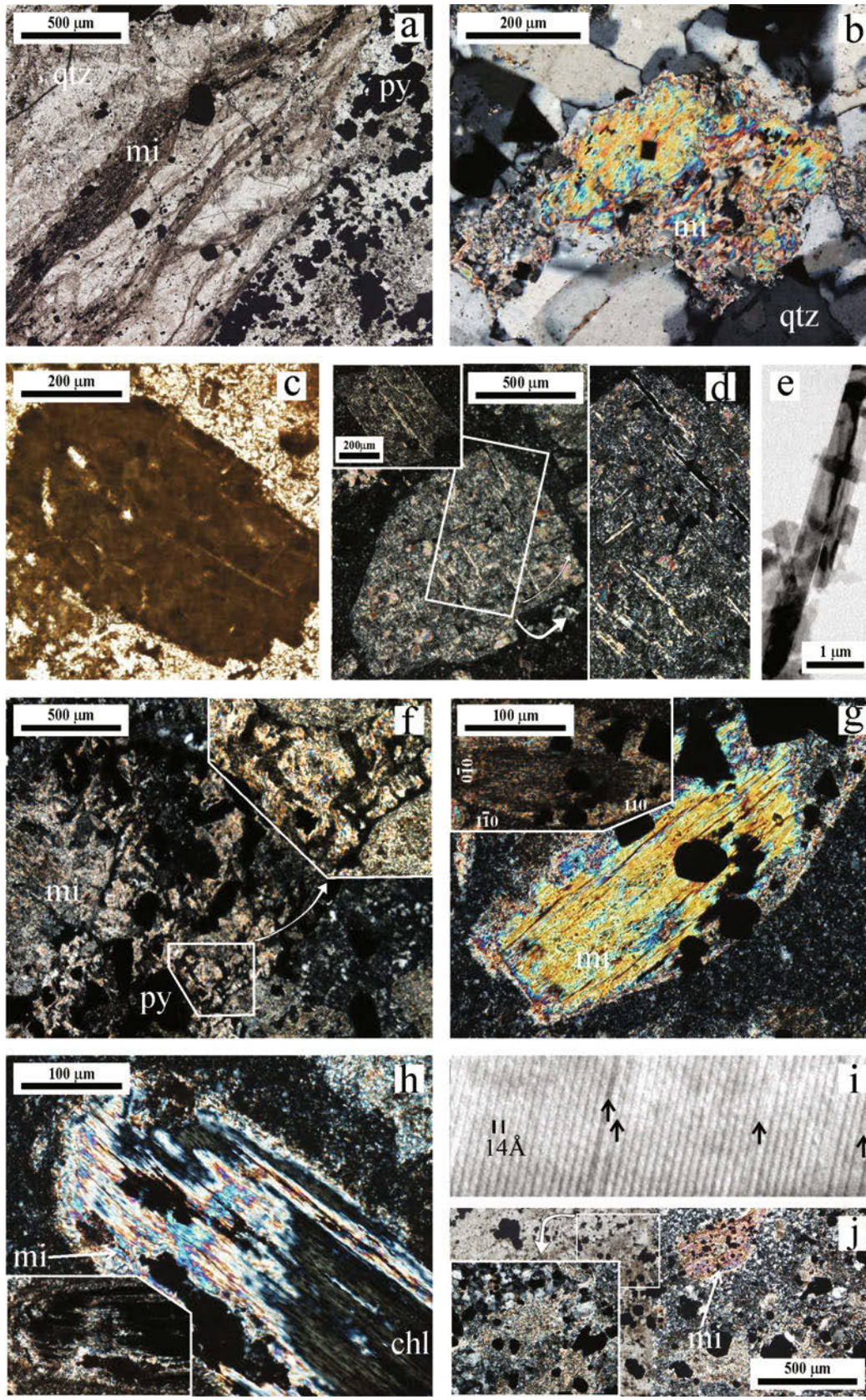

https://doi.org/10.1346/CCMN.2009.0570101 Published online by Cambridge University Press

for TEM analyses (Tables 4, 5), might correspond to polycrystalline aggregates rather than to individual crystals, because of the fine-grained character of the phyllosilicates. This makes the interpretation of the analyses very difficult, which reflects mixing of potassic illite with smectite, quartz, kaolinite, and pyrophyllite as suggested in Figure 11.

The EMPA analyses of coarse-grained phyllosilicates in the silicification area (Table 4, Figure 11) have small K (0.30−0.45 a.p.f.u.) and Al (1.57−2.27 a.p.f.u.), and large Si (3.65−4.21 a.p.f.u.) contents, which suggests the presence of interlayered smectite. The changes in backscattered images of these phyllosilicates are due to greater Si and smaller Al contents in the brighter zones than in the darker zones. This means there are domains, several micrometers in size, with greater proportions of smectite layers. Analyses by AEM, of ion-milled samples from the silicification area, have slightly greater Al (2.29−2.40), smaller Si (3.45−3.55), and similar K (0.25−0.55 a.p.f.u.) contents than achieved from EMPA analyses. This ties in with the fact that the smectite layers are very penetrative, since micrometer-sized packets with illite composition have not been detected.

The EMPA analyses of phyllosilicates from distal alteration zones are very variable, although values up 0.79 and 2.42 a.p.f.u. of K and Al, respectively (similar to those of illite from the veins and related alteration area), have been found. Therefore, illite without smectite layers at micrometer size is present in the distal alteration zone.

DISCUSSION

Characteristics of the transformation of volcanic rocks

The substrate characteristics (chemistry and crystallography) of the host rock are of great importance in phyllosilicate mineralogy (Table 1) and texture in hydrothermal alteration in relation to veins. The volcanic matrix, consisting of glass or fine-grained crystals, develops chlorite and mica and a large quantity of quartz. This non-crystalline (or fine-grained) protolith leads to both the high degree of reactivity (the volcanic matrix is the 'easiest' microdomain to alter by hydrothermal fluids) and the tendency to develop fine-grained phases. In contrast, mafic phenocrysts (hornblende and pyroxenes) mainly develop phyllosilicates (chlorite and mica). Chlorite is the main phyllosilicate which transforms mafic phenocrysts in conditions of relatively 'weak' hydrothermal alteration: chloritic alteration and propylitic alteration (the weakest alteration type). This phenomenon is due to the fact that chlorite transformation implies a minor chemical change (amphibole and pyroxenes are Fe-Mg-Si-(Al)-bearing in the same way as chlorite). In many cases, chlorite is oriented within the mafic phenocrysts (Figure 3c,d). Thus, the transformation is strongly influenced by the crystal structure of the protolith (chain structure of Si tetrahedrons) which is crystallographically similar to the layer Si tetrahedrons of chlorite. Hydrothermal fluids, which first circulate through cleavage planes, are proposed to have caused amphibole/pyroxene dissolution. Fluids were abundant, as is common in a hydrothermal system, and hot enough to enhance their reactivity. At the same time as the mafic phenocrysts were dissolving, epitaxial growth of (001) chlorite packets over (100) amphibole/pyroxene planes was occurring. Chlorite crystals with other orientations may also have nucleated, but these less abundant and smaller crystals, due to the abundance of fluid, could have dissolved. The result is that crystal growth on larger, pre-existing, oriented crystals is favored, similar to an Ostwald ripening model (*e.g.* Eberl *et al.*, 1990) but accelerated due to the fluid activity. Other types of transformation are rejected, such as the solid-state transformation of illite-smectite proposed by Altaner and Ylagan (1997). The intervention of a large quantity of fluids could easily produce dissolution processes.

Only in propylitic alteration are relics of hornblende found, while further hydrothermal alteration produces total replacement of amphiboles/pyroxenes by chlorite.

Mica also replaces mafic phenocrysts, either as phyllosilicate alone or intergrown with chlorite, mainly in zones of sericitic alteration. This mica or mica-chlorite intergrowth is usually oriented with the (001) mica planes parallel to (100) amphibole/pyroxene planes. The interpretation proposed here is that mica replaces chlorite, with an epitaxial mica growth over chlorite, and simultaneous chlorite dissolution. This occurs in a further hydrothermal alteration stage, with loss of Mg-Fe and incorporation of K in the rock. The presence of coherent one-mica layers in chlorite stacks mainly in the chloritic-sericitic alteration zones might

Figure 5 (*facing page*). Transmitted light (plane-polarized and cross-polarized light) and TEM images of mica. (a) Micro-veins of sub-microscopic mica within a quartz vein. (b) Coarse mica intergrowing with quartz. Sub-microscopic (c) and micrometer-sized (d) mica replacing a volcanic plagioclase inside hydrothermal alteration related to quartz veins. In (d), oriented crystals lie parallel to plagioclase cleavage planes and show a prismatic morphology in low-magnification TEM (e). Hornblende replaced by fine-grained, disoriented mica (f) and coherent oriented mica (g) in the hydrothermal alteration related to quartz veins. (h) Prismatic sections of mafic phenocrysts replaced by oriented chlorite and mica. (i) Lattice-fringe TEM image of chlorite (14 Å) with coherent mica layers (10 Å, marked with an arrow) in a zone of mica-chlorite intergrowth similar to (h). (j) Zone of transition between a quartz vein and the related hydrothermal alteration. Coarse-grained mica probably originated through transformation of mafic phenocrysts and fine-grained mica precedent from plagioclase transformation (within a square in the lower left corner). (A high-quality color version of this figure is available from www.clays.org/journal/JournalDeposits.html)

https://doi.org/10.1346/CCMN.2009.0570101 Published online by Cambridge University Press

Table 3. EMPA analyses of mica in the quartz veins and the related hydrothermal alteration of the Palai-Islica deposit (normalized to $O_{10}(OH)_2$).

	— Veins-neo. (n = 28) —				– Veins-tran (n = 33) –				Alteration-c.P. (n = 32)				– Alteration-f.P. (n = 6) –				Alteration-Map. (n = 12)			
Wt.%	Min	Max	Ave	S.D.	Min	Max	Ave	S.D.	Min	Max	Ave	S.D.	Min	Max	Ave	S.D.	Min	Max	Ave	S.D.
SiO_2	49.12	53.75	50.92	1.02	47.99	52.57	50.57	1.11	49.78	52.98	51.22	0.84	50.32	52.66	51.35	0.85	50.10	52.55	51.80	0.74
Al_2O_3	26.93	35.37	32.93	1.89	29.99	35.37	32.83	1.44	31.70	35.16	33.42	0.93	29.86	31.62	30.67	0.60	30.26	33.81	32.93	1.08
TiO_2	0.04	0.22	0.08	0.04	0.02	0.09	0.06	0.02	0.00	0.07	0.03	0.02	0.04	0.07	0.05	0.01	0.02	0.05	0.03	0.01
FeO	0.30	5.89	1.15	1.32	0.28	2.37	0.78	0.48	0.18	2.58	0.76	0.67	0.45	0.74	0.57	0.10	0.84	1.35	0.97	0.14
MgO	0.74	2.57	1.14	0.47	0.71	3.81	1.58	0.86	0.62	2.21	1.18	0.40	2.28	3.52	2.83	0.52	0.94	1.71	1.16	0.25
MnO	0.00	0.05	0.01	0.01	0.00	0.07	0.02	0.02	0.00	0.08	0.03	0.02	0.04	0.08	0.06	0.02	0.00	0.02	0.00	0.01
CaO	0.02	0.45	0.11	0.10	0.04	0.26	0.12	0.05	0.05	0.51	0.13	0.12	0.33	0.40	0.35	0.03	0.06	0.26	0.20	0.06
K_2O	7.94	9.95	9.10	0.44	7.41	9.73	8.81	0.68	7.35	9.17	8.47	0.63	8.34	8.86	8.62	0.20	7.30	8.77	8.05	0.43
Na_2O	0.04	0.30	0.16	0.07	0.08	0.78	0.23	0.16	0.07	1.11	0.34	0.30	0.12	0.18	0.15	0.03	0.08	0.82	0.21	0.19
F	0.00	0.33	0.18	0.08	0.10	0.37	0.21	0.05	0.00	0.28	0.06	0.08	0.03	0.15	0.10	0.04	0.00	0.14	0.05	0.05
Cl	0.00	0.09	0.01	0.02	0.00	0.05	0.02	0.01	0.00	0.05	0.02	0.01	0.00	0.00	0.00	0.00	0.00	0.06	0.02	0.01
Total	92.14	98.97	95.80	1.67	92.14	97.62	95.23	1.49	92.07	97.62	95.66	1.22	92.99	96.52	94.73	1.53	91.86	96.59	95.41	1.37
O=F	0.00	0.14	0.08	0.03	0.04	0.15	0.09	0.02	0.00	0.12	0.03	0.03	0.01	0.06	0.04	0.02	0.00	0.06	0.02	0.02
O=Cl	0.00	0.02	0.00	0.00	0.00	0.01	0.00	0.00	0.00	0.01	0.00	0.00	0.00	0.00	0.00	0.00	0.00	0.01	0.00	0.00
a.p.f.u.																				
Si	3.26	3.44	3.32	0.05	3.23	3.37	3.31	0.03	3.24	3.39	3.32	0.03	3.36	3.39	3.37	0.01	3.31	3.40	3.35	0.02
^{IV}Al	0.56	0.74	0.69	0.05	0.63	0.77	0.69	0.03	0.61	0.76	0.68	0.02	0.61	0.64	0.63	0.01	0.60	0.69	0.65	0.02
^{VI}Al	1.75	1.93	1.87	0.05	1.71	1.95	1.85	0.06	1.79	1.94	1.86	0.03	1.71	1.87	1.74	0.03	1.77	1.90	1.87	0.04
Ti	0.00	0.01	0.00	0.00	0.00	0.00	0.00	0.00	0.00	0.00	0.00	0.00	0.00	0.00	0.00	0.00	0.00	0.00	0.00	0.00
Fe	0.02	0.34	0.06	0.08	0.01	0.13	0.04	0.03	0.01	0.14	0.04	0.04	0.02	0.04	0.03	0.01	0.04	0.07	0.05	0.01
Mg	0.07	0.25	0.11	0.04	0.07	0.36	0.15	0.08	0.06	0.22	0.11	0.04	0.22	0.34	0.28	0.05	0.09	0.17	0.11	0.03
Mn	0.00	0.00	0.00	0.00	0.00	0.00	0.00	0.00	0.00	0.00	0.00	0.00	0.00	0.00	0.00	0.00	0.00	0.00	0.00	0.00
$^{VI}Ó$	1.97	2.02	2.00	0.01	2.01	2.15	2.05	0.04	1.99	2.10	2.03	0.02	2.02	2.10	2.06	0.03	2.01	2.07	2.03	0.01
Ca	0.00	0.03	0.01	0.01	0.00	0.02	0.01	0.00	0.00	0.03	0.01	0.01	0.02	0.03	0.02	0.00	0.00	0.02	0.01	0.00
K	0.68	0.82	0.76	0.03	0.60	0.82	0.74	0.06	0.60	0.77	0.70	0.05	0.69	0.74	0.72	0.02	0.62	0.74	0.67	0.04
Na	0.01	0.04	0.02	0.01	0.01	0.10	0.03	0.02	0.01	0.15	0.04	0.04	0.02	0.02	0.02	0.00	0.01	0.11	0.03	0.02
K+Na+2Ca	0.75	0.85	0.79	0.03	0.69	0.86	0.78	0.05	0.65	0.84	0.76	0.05	0.75	0.81	0.79	0.02	0.68	0.86	0.72	0.05
F	0.00	0.07	0.04	0.02	0.02	0.08	0.04	0.01	0.00	0.06	0.01	0.02	0.01	0.03	0.02	0.01	0.00	0.03	0.01	0.01
Cl	0.00	0.01	0.00	0.00	0.00	0.01	0.00	0.00	0.00	0.01	0.00	0.00	0.00	0.00	0.00	0.00	0.00	0.01	0.00	0.00

n: number of analyses; Min: minimum.; Max: maximum.; Ave: average; S.D.: standard deviation. Veins-neo: mica from the quartz veins apparently neoformed; Veins-tran: mica from the quartz veins formed primarily in hydrothermal alteration; Alteration-c.P.: relatively 'coarse' mica replacing plagioclase from the hydrothermal alteration related to quartz veins; Alteration-f.P.: 'fine' mica replacing plagioclase from the hydrothermal alteration related to quartz veins; Alteration-Map.: mica replacing mafic phenocrysts from the hydrothermal alteration related to quartz veins.

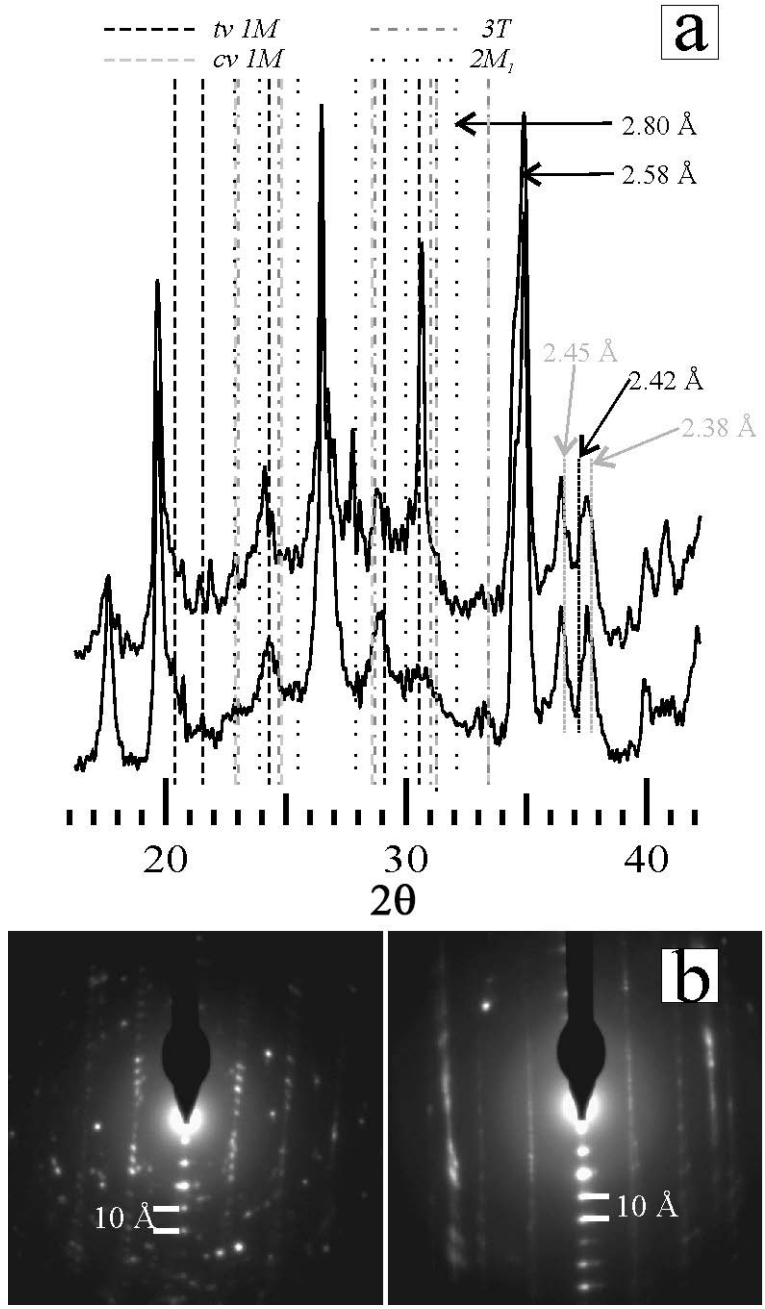

Figure 6. (a) XRD patterns of a <2 μm bulk-sample fraction from hydrothermal alteration (lower) and of mica replacing plagioclase, separated by microdrilling (upper) with vertical lines showing reflections of different polytypes according to Bailey (1980) and Moore and Reynolds (1997). The 2.58 Å and 2.80Å peaks are marked as $I_{2.80}/I_{2.58}$ and have been related to $2M/(2M+1Md)$ (Maxwell and Hower, 1967). 2.42 Å, 2.45 Å (ordered) and 2.38 Å (disordered) peaks are marked in order to estimate disorder of the $n60°$ kind (Moore and Reynolds, 1997). (b) SAED patterns of mica showing a 2*M* polytype (left) and a 3*T* polytype (right) from mica replacing plagioclase in the hydrothermal alteration and disseminated mica in a vein, respectively.

suggest mica-chlorite simultaneous precipitation (Figure 5i); this feature is, perhaps, more difficult to explain with a dissolution (chlorite)-precipitation (mica) process.

Plagioclase phenocrysts are mainly replaced by mica, due to their lack of Fe and Mg which is necessary for the formation of chlorite. This mica is finer-grained than the mica which replaces amphibole and pyroxene, reflecting a different crystallization process. The plagioclase tectosilicate structure does not normally lead to a specific mica orientation, favoring nucleation rather than crystal growth. Only occasionally could (001) and

https://doi.org/10.1346/CCMN.2009.0570101 Published online by Cambridge University Press

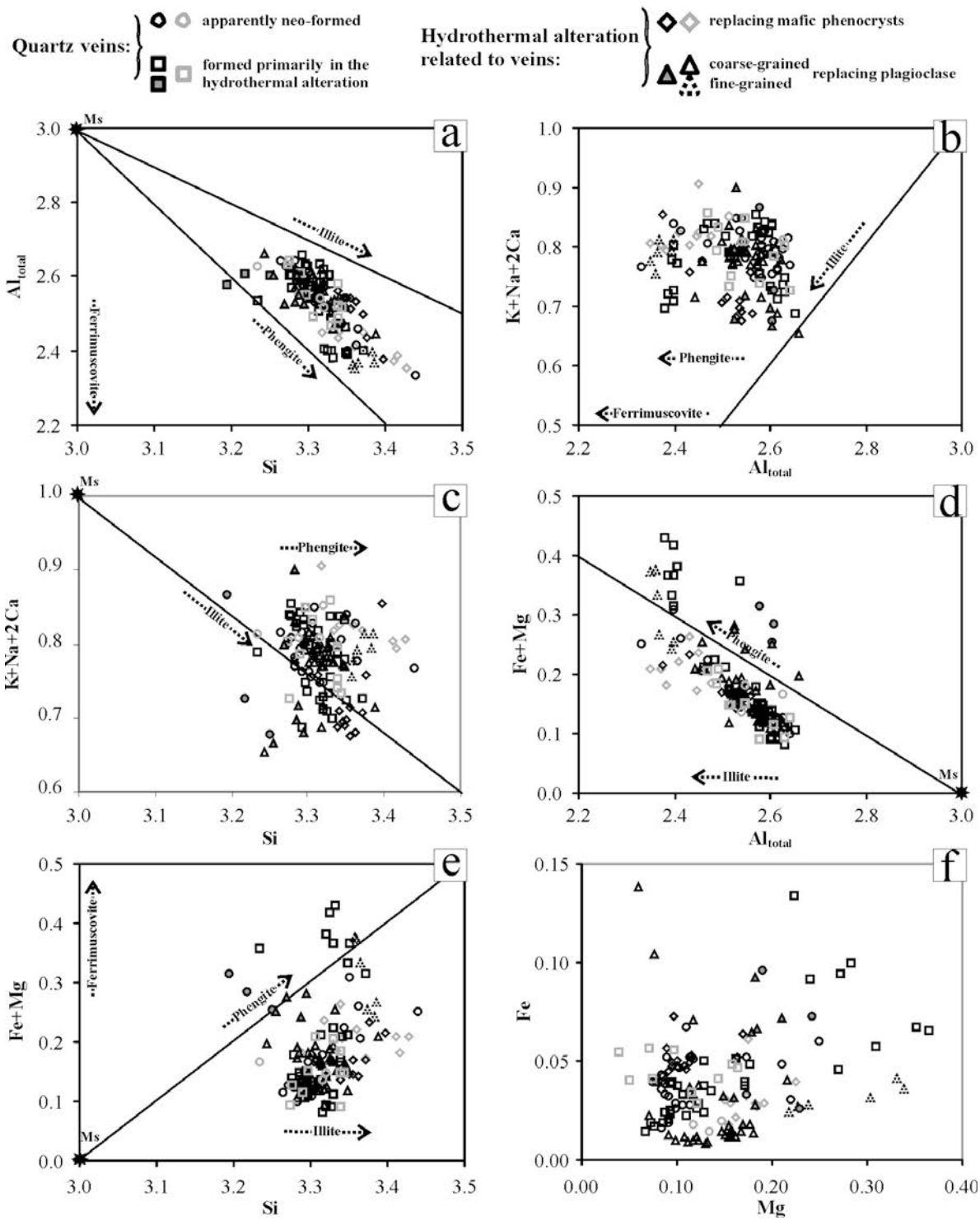

Figure 7. Binary diagrams showing compositional variations, expressed as a.p.f.u., between major elements in the different types of mica in the quartz veins and related hydrothermal alteration. The muscovite composition (Ms) and different chemical vectors are shown for comparison: illite substitution ($Si_1\square_1Al_{-1}{}^{IV}K_{-1}$), phengite substitution ($(Fe+Mg)_1Si_1{}^{VI}Al_{-1}{}^{IV}Al_{-1}$), ferrimuscovite substitution ($Fe_1^{3+IV}Al_{-1}$). EMPA-WDX analyses are plotted as black open symbols, TEM-AEM analyses as dark gray-filled symbols, and SEM-EDX analyses in gray, open symbols.

https://doi.org/10.1346/CCMN.2009.0570101 Published online by Cambridge University Press

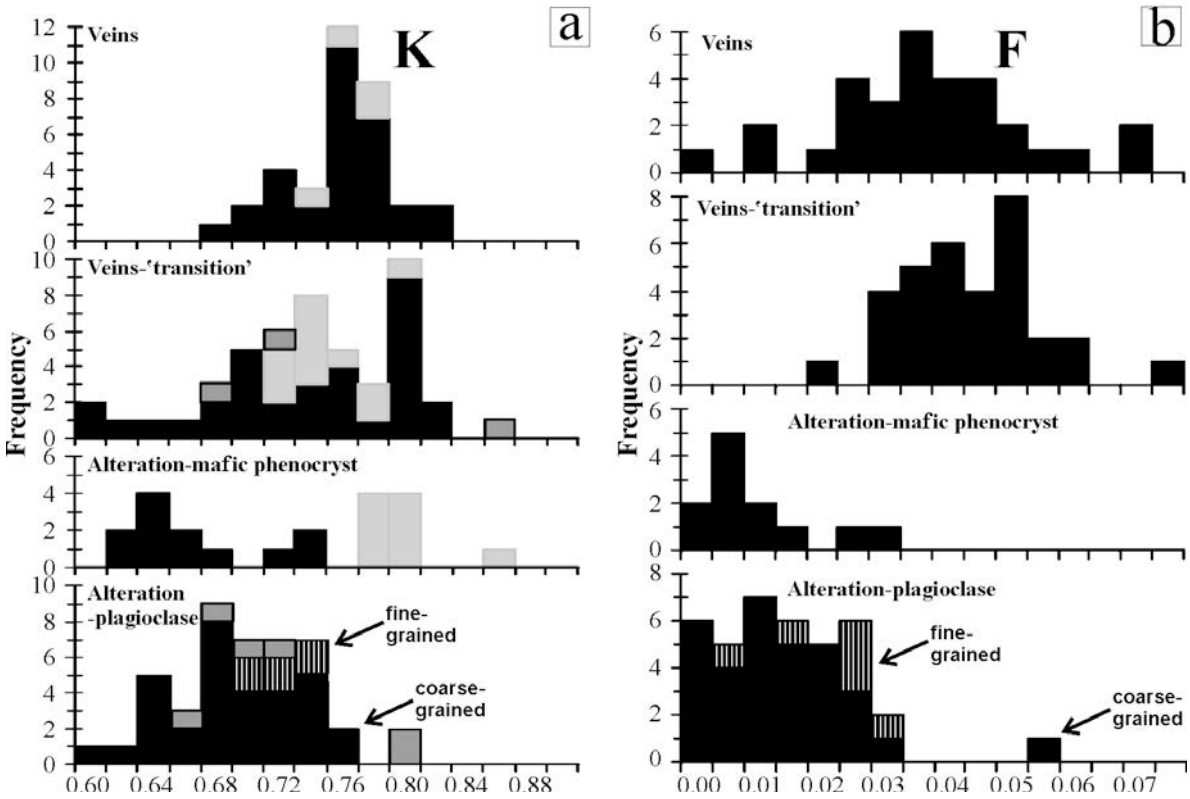

Figure 8. Frequency histograms for (a) K and (b) F content (a.p.f.u.) in the different types of mica analyzed. EMPA-WDX analyses are plotted in black columns, TEM-AEM analyses in dark gray columns, and SEM-EDX analyses in light gray columns.

(010) plagioclase cleavage planes constitute preferential locations for the growth of (001) packets of mica, with rare prismatic habit (Figure 5d,e), these being the main channel of hydrothermal fluids during the alteration processes. The size of mica crystals in plagioclase, from sub-microscopic, to 'sericite' size, could be related to the changes in the saturation state of hydrothermal fluids. Highly saturated fluids, usually linked only to sericitic alteration, could lead to sub-microscopic crystals formed in volcanic plagioclase (Figure 5c), and sometimes also simultaneously formed in mafic phenocrysts.

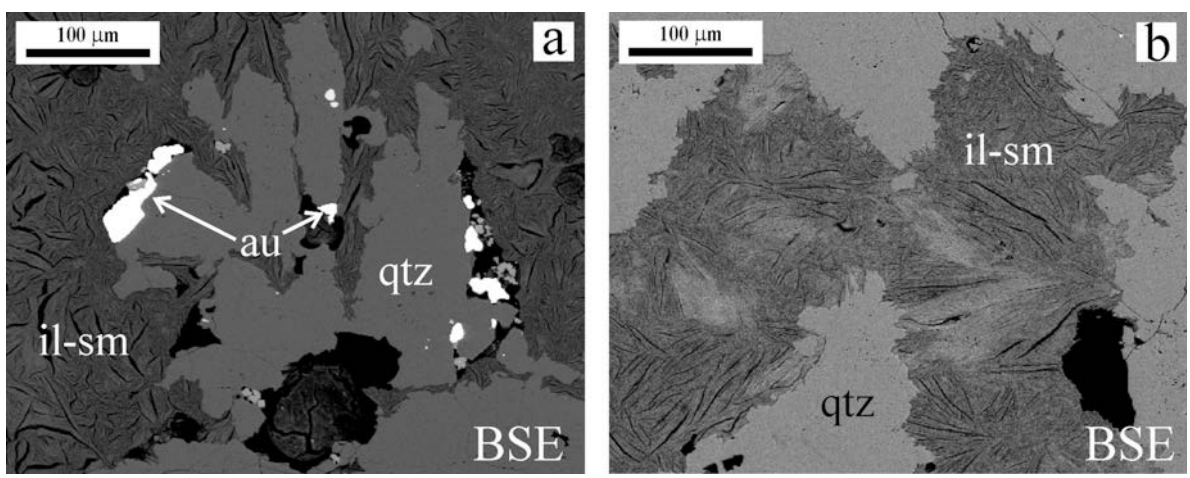

Figure 9. BSE images of illite/illite-smectite (il-sm) in the silicification. In (a), illite-smectite appears together with native gold grains (au) and quartz (qtz), while in (b) appreciable chemical zonation is visible.

https://doi.org/10.1346/CCMN.2009.0570101 Published online by Cambridge University Press

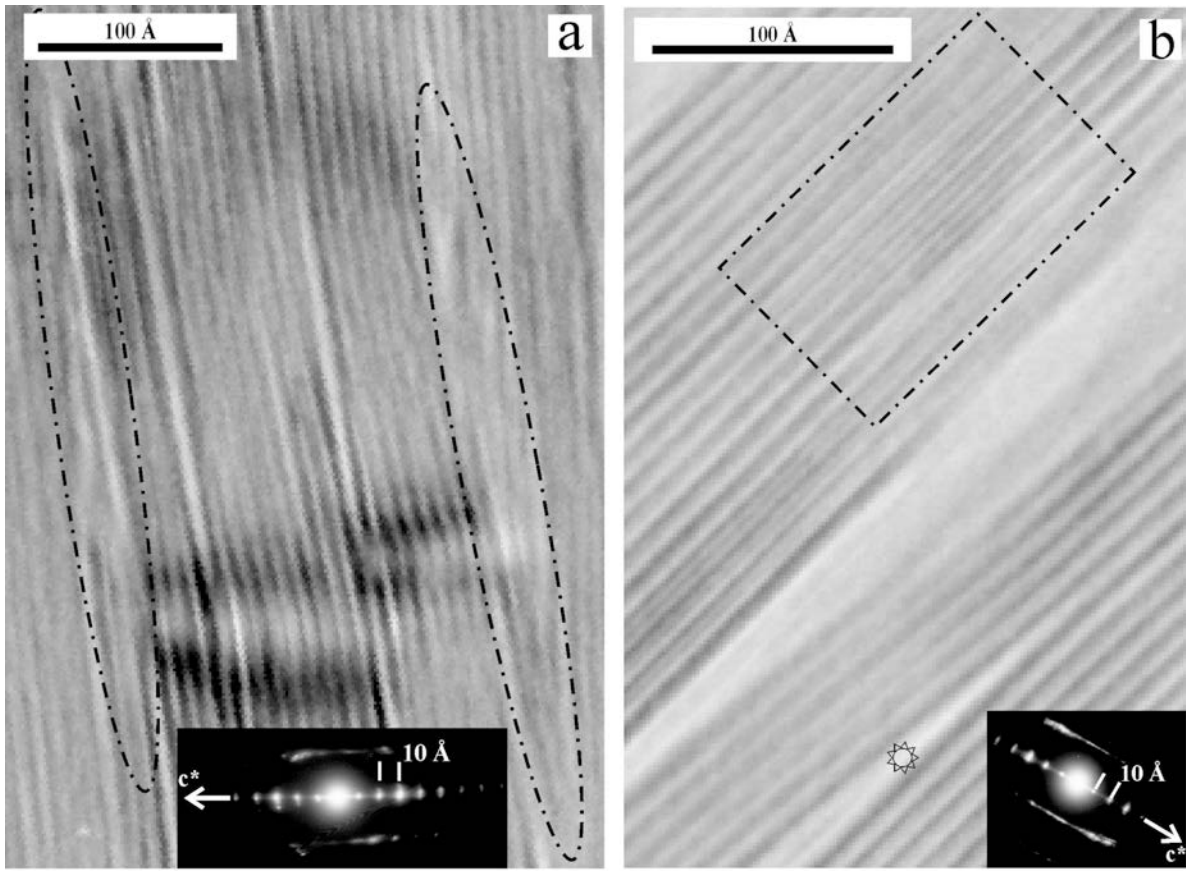

Figure 10. HRTEM (BSE) images of illite/interstratified illite-smectite with 10 Å periodicity in the silicification and relatively disordered SAED pattern. In (a) several layers in the wedge are observed to terminate (within the oval). In (b) an individual layer termination wedge is shown (*);10 Å layers splitting into 5 Å layers (see dotted rectangle), may be related to screw dislocations affecting the interstratified illite-smectite.

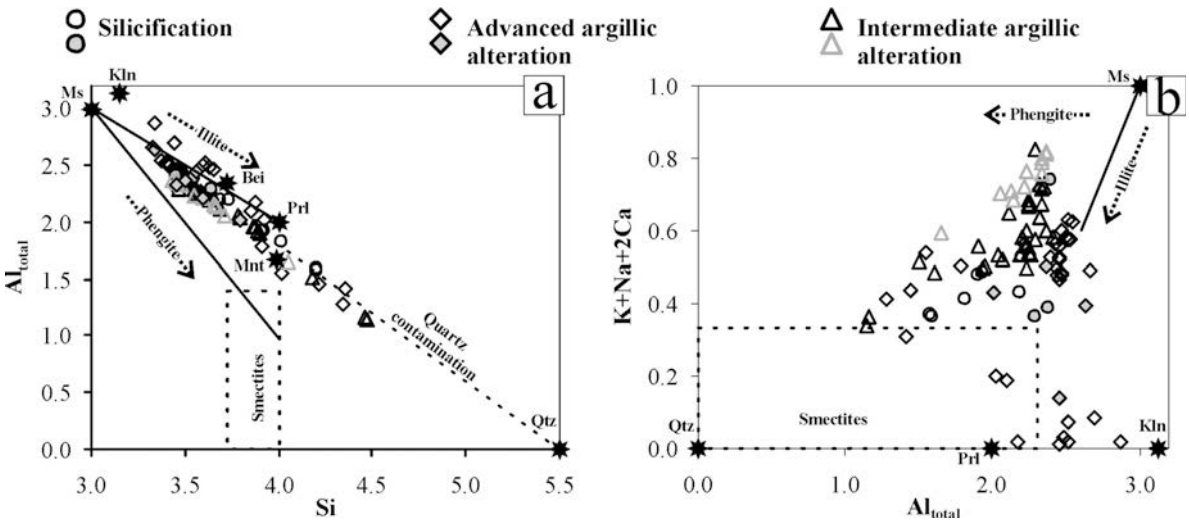

Figure 11. Binary diagrams showing compositional variations (a.p.f.u.) between Si, Al, and (K+Na+2Ca) of phyllosilicates from the silicification and related hydrothermal alteration. For comparison, the muscovite (Ms), kaolinite (Kln), pyrophyllite (Prl), beidellite (Bei), montmorillonite (Mnt), and quartz (Qtz) composition are shown, as are the illite substitution ($Si_1\square_1Al_{-1}{}^{IV}K_{-1}$) and the phengite substitution ($(Fe+Mg)_1Si_1{}^{VI}Al_{-1}{}^{IV}Al_{-1}$) chemical vectors. EMPA-WDX analyses are plotted in black, while SEM-EDX analyses are plotted in open gray symbols and TEM-AEM analyses are denoted by closed gray symbols.

https://doi.org/10.1346/CCMN.2009.0570101 Published online by Cambridge University Press

Table 4. EMPA analyses of phyllosilicates in the silicification and the related hydrothermal alteration of the Palai-Islica deposit (normalized to $O_{10}(OH)_2$).

	Silicification area (n = 8)				Advanced argillic area (n = 31)				Intermediate argillic area (n = 31)			
Wt.%	Min	Max	Ave	S.D.	Min	Max	Ave	S.D.	Min	Max	Ave	S.D.
SiO_2	49.45	64.40	59.12	5.24	41.64	62.63	50.97	4.68	47.36	66.55	53.61	4.55
Al_2O_3	19.27	28.37	24.68	3.00	14.30	35.29	27.84	6.05	10.30	30.78	25.91	4.85
TiO_2	0.00	0.02	0.01	0.01	0.00	0.20	0.03	0.06	0.01	0.38	0.06	0.06
FeO	0.11	0.19	0.15	0.02	0.02	4.16	0.56	0.81	0.17	0.97	0.44	0.18
MgO	0.31	0.51	0.41	0.06	0.04	1.57	0.81	0.48	0.33	1.84	1.11	0.49
MnO	0.00	0.02	0.01	0.01	0.00	0.03	0.01	0.01	0.00	0.07	0.02	0.02
CaO	0.24	0.48	0.33	0.08	0.03	0.82	0.24	0.21	0.03	0.85	0.26	0.21
K_2O	3.39	5.29	4.41	0.66	0.05	7.19	3.78	2.43	2.67	9.05	6.13	1.43
Na_2O	0.16	0.30	0.22	0.05	0.03	0.81	0.16	0.15	0.05	0.23	0.15	0.05
Cl	0.01	0.08	0.05	0.02	0.00	0.21	0.06	0.05	0.02	0.26	0.10	0.07
F	0.01	0.12	0.06	0.04	0.00	0.20	0.08	0.06	0.04	0.28	0.14	0.07
Total	81.55	97.12	89.44	5.21	69.01	98.04	84.54	9.24	62.36	96.37	87.95	7.90
O=F	0.01	0.05	0.02	0.02	0.00	0.09	0.03	0.03	0.02	0.12	0.06	0.03
O=Cl	0.00	0.02	0.01	0.00	0.00	0.05	0.01	0.01	0.00	0.06	0.02	0.02
a.p.f.u.												
Si	3.65	4.21	3.92	0.20	3.32	4.36	3.62	0.29	3.47	4.47	3.72	0.27
^{IV}Al	0.00	0.35	0.08	0.20	0.00	0.68	0.38	0.29	0.00	0.53	0.28	0.27
^{VI}Al	1.78	1.92	1.85	0.05	1.57	2.21	1.93	0.15	1.61	1.92	1.81	0.07
Ti	0.00	0.00	0.00	0.00	0.00	0.01	0.00	0.00	0.00	0.02	0.00	0.00
Fe	0.01	0.01	0.01	0.00	0.00	0.27	0.03	0.05	0.01	0.06	0.03	0.01
Mg	0.03	0.05	0.04	0.01	0.01	0.15	0.08	0.05	0.03	0.20	0.12	0.05
Mn	0.00	0.00	0.00	0.00	0.00	0.00	0.00	0.00	0.00	0.00	0.00	0.00
$^{VI}\Sigma$	1.61	1.97	1.85	0.13	1.80	2.23	2.04	0.09	1.80	2.06	1.96	0.07
Ca	0.02	0.03	0.02	0.01	0.00	0.06	0.02	0.02	0.00	0.06	0.02	0.02
K	0.30	0.45	0.37	0.06	0.00	0.57	0.33	0.20	0.32	0.79	0.54	0.11
Na	0.02	0.04	0.03	0.00	0.00	0.13	0.02	0.02	0.01	0.03	0.02	0.01
Interlaminae	0.37	0.53	0.45	0.06	0.01	0.63	0.39	0.21	0.34	0.83	0.58	0.10
F	0.00	0.03	0.01	0.01	0.00	0.05	0.02	0.02	0.01	0.06	0.03	0.01
Cl	0.00	0.01	0.01	0.00	0.00	0.03	0.01	0.01	0.00	0.03	0.01	0.01

n: number of analyses; Min: minimum.; Max: maximum.; Ave: average; S.D.: standard deviation. Silicification area: illite/interstratified illite-smectite from the silicification area; Advanced argillic: phyllosilicates from the advanced argillic alteration area; Intermediate argillic: phyllosilicates from the intermediate argillic alteration area.

In the hydrothermal alteration related to the silicification area, the formation of phyllosilicates implies a lesser control of rock substrate than that seen in vein-related hydrothermal alteration. In this case, a lower pH in hydrothermal fluids enhances rapid dissolution processes, avoiding significant control of volcanic

Table 5. Individual HRTEM analyses of phyllosilicates from the silicification and advanced argillic alteration (normalized to $O_{10}(OH)_2$).

	S.	S.	S.	A.A.A.	A.A.A.	A.A.A.	A.A.A.	A.A.A.	A.A.A.
Si	3.45	3.55	3.64	3.33	3.56	3.46	3.80	3.50	3.60
^{IV}Al	0.55	0.45	0.36	2.63	2.45	2.32	2.01	2.37	2.22
^{VI}Al	1.85	1.93	1.93	0.00	0.00	0.00	0.00	0.00	0.00
Fe	0.01	0.01	0.01	0.00	0.00	0.01	0.03	0.00	0.00
Mg	0.12	0.13	0.10	0.19	0.14	0.24	0.14	0.19	0.19
$^{VI}\Sigma$	1.98	2.07	2.04	2.15	2.15	2.02	1.98	2.06	2.01
Ca				0.00	0.00	0.00	0.00	0.00	0.09
K	0.55	0.39	0.25	0.39	0.14	0.60	0.38	0.50	0.39
Na	0.19	0.00	0.11	0.00	0.00	0.11	0.05	0.00	0.00
K+Na+2Ca	0.74	0.39	0.36	0.39	0.14	0.72	0.43	0.50	0.57

S.: illite/interstratified illite-smectite from the silicification analyzed following ion-milling; A.A.A.: mica/interstratified mica-smectite from the advanced argillic alteration are analyzed using a formvar Cu grid.

https://doi.org/10.1346/CCMN.2009.0570101 Published online by Cambridge University Press

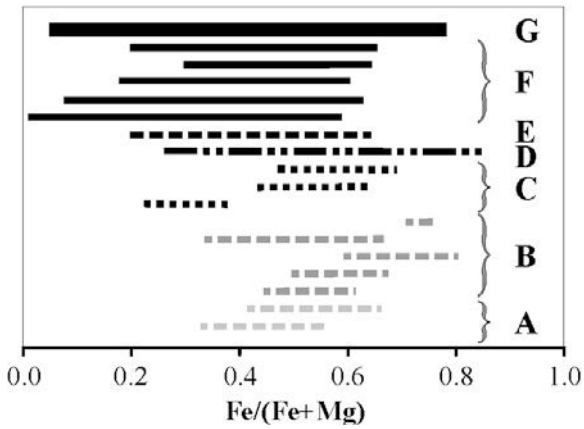

Figure 12. Variation in the relation Fe/(Fe+Mg) in chlorites from Palai-Islica and from other geological settings: (A) metabasites from New Zealand (Cooper, 1972); metapelites from New Caledonia (Black, 1975); (B) sedimentary rocks and metasedimentary rocks from the SE and NW of Spain and from Kazakhstan (Abad *et al*., 2001; 2003a; 2003b); sandstones from Texas (Boles and Franks, 1979), sediments from the Gulf Coast, USA (Ahn and Peacor, 1985); (C) Geothermal field in Los Azufres, Mexico (Cathelineau and Nieva, 1985), and Salton Sea, USA (McDowell and Elders, 1980), Pantelleria, Italy (Fulignati *et al*., 1997); (D) Hydrothermal vents in Atlantic and Pacific mid-ocean ridges (Saccocia and Gillis, 1995); (E) Altered granites (Hecht *et al*., 1999); (F) Cu veins and stratabound Cu deposits associated with basic rocks in northern Italy (Zaccarini *et al*., 2003); VHMS deposits from Canada (Kranidiotis and MacLean, 1987), from the Iberian Pyrite Belt (Sánchez España *et al*., 2000), and from Morocco (Hibti and Marignac, 2001); (G) Palai-Islica Au-Cu epithermal deposit.

substrate chemistry on the crystallization of phyllosilicates, and also avoiding epitactic phyllosilicate growth. Therefore, very fine, usually sub-microscopic phyllosilicate crystals (interstratified illite-smectite, illite, kaolinite, and pyrophyllite) are formed indistinctly over the volcanic matrix, mafic phenocrysts, and plagioclase. Nevertheless, as compared with phenocrysts, the matrix still favors quartz rather than phyllosilicate formation.

Implications of chlorite chemistry

In the Palai-Islica area, chlorites have a notable chemical variety linked to texture. Firstly, chlorites in the quartz veins and the related chloritic and sericitic alteration can be distinguished from chlorites in the propylitic alteration. The main difference is the relatively homogeneous Fe/(Fe+Mg) ratio and greater Si (Figure 4d) content in the latter than in the former. Since chlorites are widespread as a regional alteration feature, chemical analyses could be useful in detecting signs of ore-bearing-related hydrothermal activity.

Secondly, the variable chemical composition of chlorite related to the hydrothermal fluids themselves is very notable: chlorite from the quartz veins; chlorite from the chloritic and sericitic alteration; and the differences between them. The Fe/(Fe+Mg) ratio is extraordinarily broad, between 0.05 and 0.78. This is one of the broadest found in a range of environments, such as metamorphic or diagenetic/very low-grade metamorphic, and also geothermal fields and other hydrothermal deposits (Figure 12). The Fe/(Fe+Mg) variation observed in hydrothermal Palai-Islica chlorite is related to the characteristics of the hydrothermal fluids and the mechanism of chlorite formation. Chlorite precipitated directly from the hydrothermal fluids, like chlorite aggregates in the veins, has a high Fe/(Fe+Mg) ratio, reflecting the chemical composition and perhaps also the temperature of the hydrothermal fluids (*e.g.* Kranidiotis and MacLean, 1987; Saccocia and Seyfried, 1994). Nevertheless, chlorite produced by a transformation process (*i.e.* originating in the hydrothermal alteration) has a low Fe/(Fe+Mg) ratio, as its composition reflects the characteristics of hydrothermal fluids (*i.e.* composition and temperature) plus the composition of the substrate. Both mafic phenocrysts and the rock in general are relatively Mg rich, with low Fe/(Fe+Mg) ratio (Figure 4). In addition, chlorites formed, replacing phenocrysts, but subsequently incorporated within veins (Figure 3d), have an intermediate composition. This signals that a greater interaction with the fluids increases the Fe/(Fe+Mg) ratio. In other words, hydrothermal fluids produce relatively high-Fe chlorites by direct precipitation (also observable in other hydrothermal and geothermal environments, *e.g.* Kranidiotis and MacLean, 1987; Sanchez-España *et al*., 2000; Hibti and Marignac, 2001; Zaccarini *et al*., 2003), and the compositions of host rocks influence the reactant hydrothermal fluid chemistry in the host rock itself.

Si and Al, which correlate positively for ore-related hydrothermal chlorite (not in 'propylitic' chlorite, Figure 4d), are other components which clearly distinguish between chlorite from the quartz veins (more Al_{total} and ^{IV}Al, and less Si) and from the hydrothermal alteration (less Al_{total} and ^{IV}Al, and more Si). The correlation of Fe/(Fe+Mg) with Al (positive) and Si (negative) found in the hydrothermal chlorite can be explained by Tschermak substitution ($SiMg \rightleftharpoons {}^{IV}Al{}^{VI}Al$) (*e.g.* Walshe, 1986).

Octahedral vacancies are significant (0.04–0.29 a.p.f.u.) in chlorites from the veins and chloritic/sericitic alteration area, and very abundant (0.09–0.87 a.p.f.u.) in chlorites from the propylitic alteration area. Different studies have shown hydrothermal chlorite to have appreciable octahedral vacancies (*e.g.* McDowell and Elders, 1980: 0.01–0.22; Cathelineau and Nieva, 1985: 0.02–0.42; Kranidiotis and MacLean: 0.00–0.12; Fulignati *et al*., 1997: 0.15–0.25 a.p.f.u.) in comparison with metamorphic chlorite, especially high-grade (Laird, 1988). Shau *et al*. (1990) and Jiang *et al*. (1994) associated these vacancies with the existence of mica or smectite layers or inclusions. In the present study, this is the case for propylitic chlorite according to the K+Na+2Ca contents (Figure 4e) and TEM observations.

https://doi.org/10.1346/CCMN.2009.0570101 Published online by Cambridge University Press

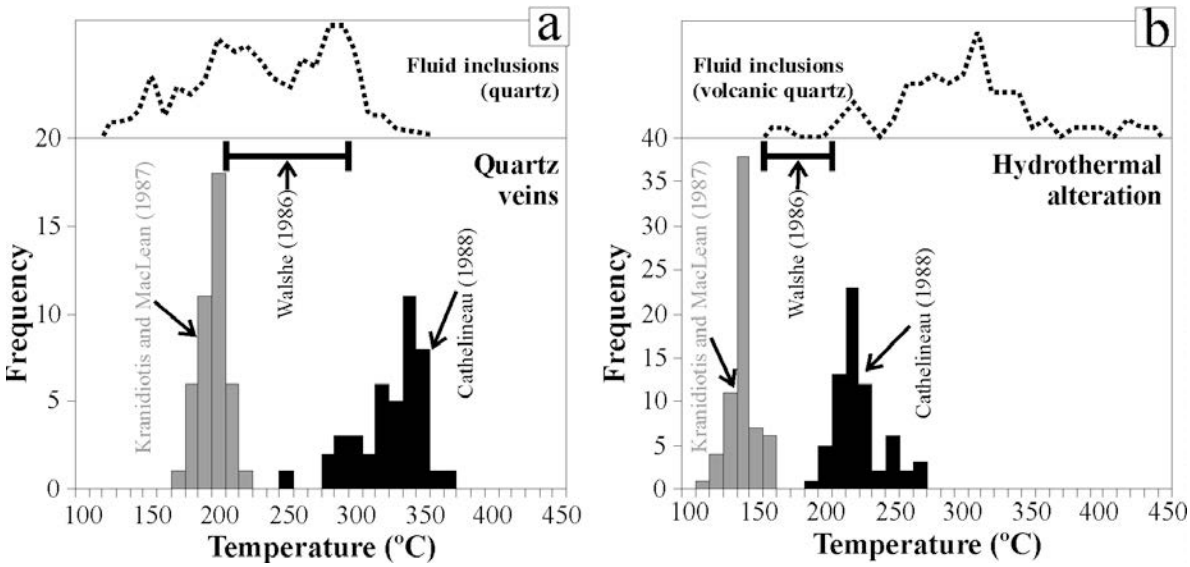

Figure 13. Frequency histograms of temperature obtained using the Kranidiotis and MacLean (1987) (gray) and Cathelineau (1988) chlorite geothermometers in (a) quartz veins with sulfides and (b) hydrothermal alteration related to quartz veins. A horizontal line shows the interval of temperatures calculated by the Walshe (1986) geothermometer for selected analyses which reflect chlorite chemical composition variability. T_h data from fluid inclusions in quartz from the veins and in volcanic phenocrysts of quartz in the hydrothermal alteration are shown for comparison. The last fluid inclusions are of secondary type, but coetaneous with hydrothermal activity. These T_h data, not in vertical scale, are from Carrillo-Rosúa (2005).

In chlorite from the veins and from chloritic/sericitic hydrothermal alteration, apparent vacancies are only partially related to a contamination effect of mica grains (Figure 4e): they could also correspond with true vacancies, the existence of which has been demonstrated by Schmidt and Livi (1999).

Finally, Mn is a relatively abundant element in the chlorite studied (up to 0.10 a.p.f.u.), more abundant than in chlorites from a sedimentary-metamorphic environment (*e.g.* Abad Martínez, 2002; Albee, 1962). It is even relatively high in comparison with other hydrothermal occurrences (*e.g.* Albee, 1962; Zaccarini *et al*., 2003). Mn in chlorite from Palai-Islica is roughly proportional to the Fe/(Fe+Mg) ratio (Figure 4b), reaching greater values in chlorites from the veins. Therefore its concentration has much to do with ore-fluids. The association of Mn-bearing minerals with hydrothermal ore-bearing activity has also been highlighted in carbonate phases (Carrillo-Rosúa *et al*., 2005).

Implications of mica chemistry

Microprobe analyses of mica of different textural kinds show interlayer charge between +0.65 and +0.86 p.f.u. Therefore, a large number of analyses correspond to an illite-smectite composition (charge of <0.75 according to Newman and Brown, 1987). Nevertheless, the numerous XRD patterns do not show modifications of 001 peaks after ethylene glycol solvation. The interlayer composition is dominantly potassic, while the paragonitic and margaritic component is very low (generally <0.05 and 0.02 a.p.f.u. of Na and Ca, respectively). In the octahedral sheet, meanwhile, the Fe+Mg content (0.08−0.42 a.p.f.u.) is notably large, the octahedral charge usually being between 2 and 2.05. The Fe content is almost always less than the Mg content and usually very similar for each textural mica type, the Mg content being the most variable (Figure 7f). Therefore, the Fe/(Fe+Mg) ratio is variable, although in a lower range than in chlorite (mainly between 0.1 and 0.4).

Therefore, the composition of this potassic octahedral mica could be explained by illitic ($Si_1\square_1Al^{IV}_{-1}K_{-1}$) and phengitic ($(Fe+Mg)_1Si^{VI}_1Al^{IV}_{-1}Al_{-1}$) substitution vectors. The F content in this mica is small, though significant (up to 0.08 a.p.f.u.). Some variations are present between different textural mica types. Mica from the veins usually has a smaller illitic component and more F than mica from the chloritic and sericitic alteration areas (Figures 7a, 8b). The differences in the illitic component could be related to 'disequilibrium' and even to formation temperature. Muscovite is known *sensu stricto* to have begun its formation in a very low-grade metamorphic environment, in epizone conditions, ~200ºC (*e.g.* Abad Martínez, 2002). In the Palai-Islica mica system, however, no muscovitic composition has been found at temperatures as high as 300ºC (Morales-Ruano *et al*., 2000; Carrillo-Rosúa *et al*., 2003a). Similar non-muscovitic composition has been found in other Au epithermal deposits, such as Red Mountain (USA) or El Dorado (Chile). Even in these cases, more phengitic and illitic composition appears, but lower formation temperatures are also suggested (Bove *et al*., 2002; Carrillo-Rosúa *et al*., 2008b).

https://doi.org/10.1346/CCMN.2009.0570101 Published online by Cambridge University Press

A complementary view could be deduced from the polytypism of Palai-Islica mica: the existence of different polytypes including 1*M* polytype mainly in the hydrothermal alteration domain (Figure 6), could suggest 'variable disequilibrated conditions.'

Mica in the veins could be less disequilibrated than mica in the hydrothermal alteration on account of a greater fluid/rock ratio in the former compared with the latter, rather than being due to the time factor, given that they could be formed during the same time interval. A greater temperature for mica from the veins could be another factor. Higher temperatures in other environments, such as very low-grade metamorphism, led to lower and more homogeneous illitic levels (*e.g.* Lee *et al*., 1986; López Munguira and Nieto, 2000; Abad Martínez, 2002). This aspect will be discussed in the specific geothermometry section below. Ore-forming fluids are clearly responsible for the introduction of F, as is also suggested by apatite chemistry (Carrillo Rosua *et al*., 2005). Therefore, F in mica could be used as a 'chemical vector' related to the 'intensity' of hydrothermal activity in a certain zone of the Palai-Islica deposit, and by extrapolation for other similar hydrothermal areas.

Further chemical differences are also linked to specific mica textural groups. 'Coarse' mica, replacing volcanic plagioclase, has greater K and Al contents, along with smaller Si, and generally smaller Fe contents (suggesting a greater illitic level), than mica which replaces amphibole and pyroxene. Microcrystalline mica, replacing volcanic plagioclase, has relatively high K, but also high Si and Mg, and low Al and Fe, suggesting contamination of the analyses with some submicroscopic chlorite. The cause for these chemical differences could, again, be related to kinetic problems and the types of crystallization processes. Mica that replaces plagioclase crystals is smaller in size than mica replacing mafic phenocrysts, having a greater specific surface area to equilibrate with the hot hydrothermal fluids, and is, therefore, less 'disequilibrated,' *i.e.* less illitic in its composition. Moreover, in mica replacing amphiboles and pyroxenes, mica replaces chlorite by chlorite dissolution, epitactic mica crystallization favoring an Fe/(Fe+Mg) ratio similar to that of the chlorite which it replaces.

Finally, mica crystals in the veins which represent xenocrysts from the hydrothermal alteration have a relatively large F content compared with mica crystallized directly in the vein, reflecting a longer 'history' of interaction with the F-bearing hydrothermal fluids.

Geothermometry

Despite the questionable validity of chlorite thermometry (*e.g.* Shau *et al*., 1990; Jiang *et al*., 1994), the equations of Kranidiotis and MacLean (1987) and Cathelineau (1988) have been applied tentatively and the results plotted in Figure 13. Significantly, the temperatures obtained by chlorite geothermometry for the veins are 75−150ºC higher than in the hydrothermal alteration. However, the fluid inclusion data do not show greater temperatures of homogenization (T_h) in the veins than in the hydrothermal alteration. In fact, they even show the opposite: the same mode value, but a greater range reaching lower T_h (Carrillo-Rosúa, 2005). The obvious conclusion is that the empirical chlorite geothermometers do not work in the case of the Palai-Islica deposit. Alternatively, they could be deemed to have qualitative use within the Palai-Islica deposit. Empirical observations (*e.g.* Kranidiotis and MacLean, 1987; Cathelineau, 1988) and thermodynamic calculations for high-variance assemblages (Vidal *et al*., 2005) could support the second alternative.

The measured fluid inclusions in the hydrothermal alteration are secondary with respect to the volcanic quartz phenocrysts and are probably representative of 'peak' conditions of the hydrothermal system. Under these 'peak' conditions, fluids have enough energy to crack quartz phenocrysts and cause the fluid inclusions, while at lower temperatures hydrothermal fluids do not have enough energy and do not produce fluid inclusions. In the quartz veins, however, fluid inclusions better represent the full range of hydrothermal fluid activity since quartz is crystallizing and fluid inclusions are primary. Therefore, in the hydrothermal alteration the average temperature during the activity of the hydrothermal system possibly could be lower than in the veins, although the peak (or peaks) would be the same. This would be in accordance with the chlorite geothermometry but also with the illitic component of mica (related in some way to temperature; Cathelineau, 1988). Lower average temperatures in the volcanic, hydrothermally altered rocks than in the veins seems reasonable and could be related to a drop in temperature of the hydrothermal fluids after leaving the main conduit channels (veins) and circulating through the host rocks (hydrothermal alteration). Alternatively, it could be related to a cooling of the fluids in the pores and cracks in the host rock in contact with neoformed minerals (and therefore with mineral-fluid interaction and possibly to modify mineral composition) while the veins are sealed by mineralization processes.

Alteration typology and genetic implications in ore deposition

Development of pervasive halos of hydrothermal alteration by the two different gold-bearing mineralizations, but with significant mineral differences, is noteworthy, especially in relation to phyllosilicate phases (Figure 2).

The quartz veins with sulfides (the most important form of mineralization) are polymetallic (Cu, Zn, Pb, Au, Ag...) and sulfur rich. Veins and their related hydrothermal alteration are characterized by dioctahedral mica and chlorite as phyllosilicate phases. This

https://doi.org/10.1346/CCMN.2009.0570101 Published online by Cambridge University Press

alteration could be defined as sericitic in zones where mica is the dominant mineral phase, and chloritic when chlorite is abundant (with the possible presence of albite). The former represents a greater intensity of hydrothermal alteration. This means that the mineralization type and associated alteration are related to hydrothermal fluids, which are base and precious metal-bearing and of near-neutral pH. Furthermore, they have temperatures of 150–300ºC according to fluid inclusion studies (Morales-Ruano *et al*., 2000). These features coincide with an intermediate-sulfidation hydrothermal system (Hedenquist *et al*., 2000).

The silicification is a type of mineralization which is poor in sulfide sulfur and base metals, although it contains high grades of gold. It develops a very different hydrothermal alteration. The core consists of silicification containing ore gold-bearing mineralization. The silicification is surrounded by an advanced argillic envelope, consisting mainly of pyrophyllite, kaolinite (with low disorder), illite, and quartz. An outer-intermediate argillic envelope consists of illite and interstratified illite-smectite and quartz.

This silicification + advanced argillic alteration represents an intense leaching of the volcanic rock with lixiviation of the different cations present in the rock with the exception of Si + Al (argillic alteration), and only Si (silicification) in more extreme conditions. Very low-pH fluids are considered to be compatible with the formation of the advanced phyllosilicate assemblage (*e.g.* Reyes, 1990; Fialips *et al*., 1998) and are responsible for this extreme lixiviation process, consistent with a high-sulfidation hydrothermal environment (*e.g.* Hedenquist *et al*., 2000). The transition of silicification to advanced argillic envelopes is explained by progressive fluid modification due to rock interaction in the movement of hydrothermal fluids from their feeder conduits, situated in silicification zones, to external areas. This progressive fluid modification would imply an increase in pH level and a fall in temperature, according to the mineralogical zonation; kaolinite located in outer zones, as compared with pyrophyllite, is of lower-temperature formation (*e.g.* Browne, 1978; Henley and Ellis, 1983; Reyes, 1990). However, available fluid-inclusion data (Carrillo-Rosúa, 2005) do not suggest appreciable changes in temperature of homogenization between silicification, advanced argillic alteration with pyrophyllite, and advanced argillic alteration with kaolinite. This T_h, measured in secondary fluid inclusions in quartz volcanic phenocrysts, is mainly 260±30ºC and seems to be too high for the presence of kaolinite, but appropriate for pyrophyllite formation (Berman, 1988; Bjorkum and Walderhaugh, 1993). In hydrothermal systems kaolinite is assumed to occur at temperatures not >200ºC (*e.g.* Browne, 1978; Henley and Ellis, 1983; Reyes, 1990), while in diagenetic and/or very low-grade metamorphic sequences, kaolinite transforms to become dickite at temperatures of 130ºC (*e.g.* Ehrenberg *et al*., 1993; Lázaro *et al*., 2003). This apparent inconsistency between fluid inclusion and mineralogical data could be explained by kinetic effects. Hot hydrothermal fluids interact more (more fluids + more time) with the rock in the inner zone surrounding fluid conduits (*i.e.* the silicification and the inner zones of the advanced argillic envelope) than in outer zones of the advanced argillic envelope, where kaolinite appears.

The intermediate argillic alteration area characterized by illite and interstratified illite-smectite represents a less intense alteration and lixiviation area caused by higher-pH fluids, in comparison to the silicification and advanced argillic alteration zones. Its origin is related to the same hydrothermal fluids which produce the silicification + advanced argillic envelope, although they are neutralized due to rock interaction, and the fluid/rock ratio may also be less.

As its presence is inconsistent with temperatures of >200ºC (*e.g.* Merriman and Peacor, 1991), interstratified illite-smectite in the silicification and in the advanced argillic envelope could be related to a second stage in the formation of the silicification + argillic envelope. This second stage would be of lower temperature (<200ºC) and higher pH with respect to the first stage, and, very significantly, is responsible for the gold mineralization. This is deduced from the association of native gold and directly precipitated interstratified illite-smectite aggregates (no illites without smectite interstratification have been found). This illite-smectite is very illite-rich, which could suggest a lower formation temperature, although still close to 200ºC (*e.g.* Merriman and Peacor, 1991).

The interstratified illite-smectite in the intermediate argillic alteration zone could have been precipitated in the first hydrothermal stage due to a higher pH and lower temperature and fluid/rock ratio conditions in this more external area, but also in the second-stage hydrothermal event.

Surrounding the chloritic and sericitic alteration zones (related to the quartz veins), as well as argillic and silicification areas, is a zone of weak alteration that could be defined as propylitic. In this area, plagioclase phenocrysts could remain unaltered or with only some phyllosilicate crystals (*i.e.* illite and interstratified illite-smectite), while mafic phenocrysts are usually totally or partially altered to chlorite. The presence of epidote and calcite (rather than dolomite, which appears occasionally in chloritic and sericitic alteration areas, Carrillo-Rosúa *et al*., 2005) is also usually a characteristic feature.

Outside the Palai-Islica deposit, propylitic alteration becomes a regional alteration feature, with the disappearance of epidote. This propylitic alteration represents an area with a low infiltration rate of hydrothermal fluids, a low fluid/rock ratio, and the presence of other cool meteoric regional fluids. These are responsible for the 'regional alteration' and, mixed with a certain

https://doi.org/10.1346/CCMN.2009.0570101 Published online by Cambridge University Press

proportion of hydrothermal fluids, they give rise to propylitic alteration. Thus, these rocks have suffered a minor chemical change, reflected in the chlorite chemistry, with the Fe/(Fe+Mg) ratio equal to the mafic phenocrysts.

CONCLUSIONS

Phyllosilicates are widespread phases among the mineralization and hydrothermal alteration zones in the Palai-Islica deposit. Two different phyllosilicate (alterations and/or neo-formed) assemblages have been distinguished and related to two different kinds of ores: mica and chlorite associated with polymetallic gold and silver-rich veins; mica, interstratified illite-smectite, and kaolinite and pyrophyllite associated with gold dissemination in the silicification. The former, defined as chloritic and sericitic, is caused by near-neutral, highly metal-rich hydrothermal fluids, while the latter is produced by acidic, gold-bearing hydrothermal fluids in which a neutralization process and kinetic aspects determine a certain mineral zonation pattern (silicification → advanced argillic → intermediate argillic). Noteworthy here is that gold precipitation occurs at temperatures $\leqslant$200ºC, which is less than that responsible for the main hydrothermal alteration/silification formation stage. This is due to its association with interstratified illite-smectite. A propylitic halo (chlorite, epidote, calcite-bearing) encloses the other alteration zones. Therefore, two epithermal environments have been identified in the same deposit: intermediate-sulfidation and high-sulfidation.

The advanced and intermediate argillic alteration zones develop very fine-grained phyllosilicates, more concentrated in volcanic phenocrysts with respect to the matrix. This is related to a rapid, enhanced dissolution process due to the low pH of the hydrothermal fluids. In the chloritic and sericitic alteration zones, coarse-grained phyllosilicates (mainly inside mafic phenocrysts due to their anisotropic structure) and epitactic crystallization features (mafic phenocrysts → chlorite → mica) appear, suggesting a weaker dissolution process due to the near-neutral conditions of the hydrothermal fluids.

Chlorite and mica show a very wide compositional range. Chlorite chemistry, mainly the Fe/(Fe+Mg) ratio and the Si and Al contents, distinguishes between origins related to high- or low-temperature fluids (*i.e.* chlorite of propylitic/regional alteration origin). In addition, these elements differ strongly in concentrations between chlorites in the hydrothermal alteration zone and that directly precipitated in the veins, thus suggesting different genetic conditions (*i.e.* fluid/rock ratio, influence of substrate, temperature, etc.). Mica also manifests some chemical composition differences according to its location: veins or hydrothermal alteration, the latter being richer in illitic component and poorer in F, directly related to ore fluids. The composition and polytypism of mica suggest that equilibrium conditions were not reached during hydrothermal activity.

Although chlorite thermometry is said to be invalid (*e.g.* Jiang *et al*., 1994), temperatures calculated with the empirical geothermometers available could be useful in estimating a range of formation temperatures, to suggest vectors of temperature variation in a hydrothermal deposit, or, when combined with other methods such as fluid inclusions, to give clues about the thermal evolution of a hydrothermal system.

ACKNOWLEDGMENTS

This work was supported by the Spanish projects CGL-2006-02594/BTE (Ministry of Education (MEC) and Science and FEDER), and RNM-732 (Junta de Andalucía). J. Carrillo-Rosúa is grateful for a postdoctoral grant from MEC. The authors are also very grateful to Fernando de la Fuente Consultores S.L. for providing drill-core samples and for help during field work, and to technical staff of the 'Centro de Instrumetación Científica' of the University of Granada for assistance with the TEM, SEM, and EMPA work. The manuscript was improved significantly by helpful suggestions and critiques by Dr Saccocia and another, anonymous reviewer. Editors Derek C. Bain and W. Crawford Elliott are thanked for their constructive comments and encouragement.

REFERENCES

Abad Martinez, M.I. (2002) Procesos diagenéticos y metamórficos de grado muy bajo en rocas clásticas: evolución textural y química de los filosilicatos. PhD thesis, University of Granada, Spain.

Abad, I., Mata, P., Nieto, F., and Velilla, N. (2001) The phyllosilicates in diagenetic-metamorphic rocks of the South Portughese Zone, southwestern Portugal. *The Canadian Mineralogist*, **39**, 1571–1589.

Abad, I., Nieto, F., and Gutiérrez-Alonso, G. (2003a) Textural and chemical changes in slate-forming phyllosilicates across the external-internal zones transition in the in the low-grade metamorphic belt of the NW Iberian Variscan Chain. *Schweizerische Mineralogische und Petrographische Mitteilungen*, **83**, 63–80.

Abad, I., Gutiérrez-Alonso, G., Nieto, F., Gertner, I., Becker, A., and Cabero, A. (2003b) The structure and the phyllosilicates (chemistry, crystallinity and texture) of Talas ala-Tau (Tien Shan, Kyrgyz Republic): comparison with more recent subduction complexes. *Tectonophysics*, **365**, 103–127.

Ahn, J.H. and Peacor, D.R. (1985) Transmission electron microscopic study of diagenetic chlorite in Gulf Coast argillaceous sediments. *Clays and Clay Minerals*, **33**, 228–236.

Albee, A.L. (1962) Relationships between the mineral association, chemical composition and physical properties of the chlorite series. *American Mineralogist*, **47**, 851–870.

Altaner, S.P. and Ylagan, R. (1997) Comparison of structural models of mixed-layer illite/smectite and reaction mechanisms of smectite illitization. *Clays and Clay Minerals*, **45**, 517–533.

Arribas, A. Jr. and Tosdal, R. (1994) Isotopic composition of Pb in ore-deposits of the Betic Cordillera, Spain. Origin and relationship to other European deposits. *Economic Geology*, **89**, 1074–1093.

Arribas, A., Cunningham, C.G., Rytuba, J.J., Rye, R.O., Kelly, W.C., Podwysocki, M.H., McKee, E.H., and Tosdal, R.M.

(1995) Geology, geochronology, fluid inclusions, and isotope geochemistry of the Rodalquilar gold alunite deposit, Spain. *Economic Geology*, **90**, 795–822.

Bailey, S.W. (1980) Structure of layer silicates. Pp. 1–123 in: *Crystal Structures of Clay Minerals and their X-ray Identification* (G.W. Brindley and G. Brown, editors). Mineralogical Society, Monograph **5,** London.

Bellon, H., Bordet, P., and Montenat, C. (1983) Chronologie du magmatisme Néogène des Cordillères Bètiques (Espagne mèridionale). *Bulletin de la Société Géologique de France*, **25**, 205–217.

Berman, R.G. (1988) Internally consistent thermodynamic data for stoichiometric minerals in the system Na_2O-K_2O-CaO-MgO-FeO-Fe_2O_3-Al_2O_3-SiO_2-TiO_2-H_2O-CO_2. *Journal of Petrology*, **29**, 445–522.

Bjorkum, P.A. and Walderhaugh, O. (1993) A model for the effect of illitization on porosity and quartz cementation sandstones. *Journal of Sedimentary Petrology*, **63**, 1089–1091.

Black, P.M. (1975) Mineralogy of New Caledonia metamorphic rocks: IV. Sheet silicates from the Ouegoa District. *Contributions to Mineralogy and Petrology*, **49**, 269–284.

Boles, J.R. and Franks, S.G. (1979) Clay diagenesis in Wilcox sandstones of southwest Texas: implications of smectite diagenesis on sandstones cementation. *Journal of Sedimentary Petrology*, **49**, 269–284.

Bove, D.J., Eberl, D.D., McCarty, D.K., and Meeker, G.P. (2002) Characterization and modelling of illite crystal particles and growth mechanism in a zoned hydrothermal deposit, Lake City, Colorado. *American Mineralogist*, **87**, 1546–1556.

Browne, P.R.L. (1978) Hydrothermal alteration in active geothermal fields. *Annual Review of Earth and Planetary Sciences*, **6**, 229–250.

Caballero, E., Reyes, E., Linares, J., and Huertas, F. (1985) Hydrothermal solutions related to bentonite genesis, Cabo de Gata Region, Almería, SE Spain. *Mineralogica et Petrographica Acta*, **29**, 187–196.

Caballero, E., de Cisneros, C.J., Huertas, F.J., Huertas, F., Pozzuoli, A., and Linares, J. (2005) Bentonites from Cabo de Gata, Almeri'a Spain: A mineralogical and geochemical overview. *Clay Minerals*, **40**, 463–480.

Carrillo-Rosúa, F.J. (2005) El depósito epitermal de oro-cobre Palai-Islica (Carboneras, Almería). Mineralogía, geoquímica y metalogenia. PhD thesis, Univ. Granada., Spain.

Carrillo-Rosúa, F.J., Morales-Ruano, S., and Fenoll-Hach-Alí, P. (2002) The three generations of gold in the Palai-Islica epithermal deposit, southeastern Spain. *The Canadian Mineralogist*, **40**, 1465–1481.

Carrillo-Rosúa, F.J., Morales-Ruano, S., Boyce, A.J., and Fallick, A.E. (2003a) High and intermediate sulphidation environment in the same hydrothermal deposit: the example of Au-Cu Palai-Islica deposit, Carboneras (Almería). Pp. 445–448 in: *Mineral Exploration and Sustainable Development* (D.G. Eliopoulos *et al*., editors). Millpress, Rotterdam, The Netherlands.

Carrillo-Rosúa, F.J., Morales Ruano, S., and Fenoll Hach-Alí, P. (2003b) Iron sulphides at the epithermal gold-copper deposit of Palai-Islica (Almería, SE Spain). *Mineralogical Magazine,* **67**, 1059–1080.

Carrillo-Rosúa, F.J., Morales Ruano, S., Fenoll Hach-Alí, P., Boyce, A.J., and Fallick, A.E. (2003c) Génesis de la barita de Las Herrerías y Sierra Almagrera. *Boletín de la Sociedad Española de Mineralogía*, **26-A**, 159–160.

Carrillo-Rosúa, F.J., Morales Ruano, S., Fenoll Hach-Alí, P., Morata Céspedes, D., Belmar, M., Boyce, A.J., and Fallick, A.E. (2005) Mineralogical and chemical features of gangue phases in relation to hydrothermal mineralization and their host rocks. Pp. 1057–1060 in: *Mineral Deposit Research: Meeting the Global Challenge* (Y. Chen *et al*., editors). Millpress, Rotterdam, The Netherlands.

Carrillo-Rosúa, F.J., Morales Ruano, S., and Fenoll Hach-Alí, P. (2008a) Textural and chemical features of sphalerite from the Palai-Islica deposit (SE Spain): implications for ore genesis and color. *Neues Jahrbuch für Mineralogie – Abhandlungen*, **185/1**, 49–64.

Carrillo-Rosúa, F.J., Morales-Ruano, S., Morata, D., Boyce, A.J., Fallick, A.E. Belmar, M., and Fenoll Hach-Alí, P. (2008b) Mineralogy and geochemistry of El Dorado epithermal gold deposit, El Sauce district, central-northern Chile. *Mineralogy and Petrology*, **92**, 341–360.

Cathelineau, M. (1988) Cation site occupancy in chlorites and illites a function of temperature. *Clay Minerals*, **23**, 471–485.

Cathelineau, M. and Nieva, D. (1985) A chlorite solid solution geothermometer. The Los Azufres (Mexico) geothermal system. *Contributions to Mineralogy and Petrology*, **91**, 235–244.

Cliff, G. and Lorimer, G.W. (1975) The quantitative analysis of thin specimens. *Journal of Microscopy*, **103**, 203–207.

Cooper, A.F. (1972) Progressive metamorphism of metabasic rocks form the Haast schist group of southern New Zeland. *Journal of Petrology*, **13**, 457–492.

Dewey, J.F. (1988) Extensional collapse of orogens. *Tectonics*, 7, 1123–1140.

Eberl, D.D., Środoń, J., Kralik, M., Taylor, B.E., and Peterman, Z.E. (1990) Ostwald ripening of clays and metamorphic minerals. *Science*, **248**, 474–477.

Ehrenberg, S.N., Aagaard, P., Wilson, M.J., Fraser, A.R., and Duthie, M.L. (1993) Depth-dependent transformation of kaolinite to dickite in sandstones of the Norwegian continental shelf. *Clay Minerals*, **28**, 325–352.

Fernández Soler, J.M. (1996) El vulcanismo calc-alcalino en el Parque Natural de Cabo de Gata-Nijar (Almería). Estudio volcanológico y petrológico. PhD thesis, Univ. Granada, Sociedad Almeriense Historia Natural, Spain.

Fialips, C.I., Petit, S., Decarreau, A., and Beaufort, D. (1998) Effects of temperature and pH on the kaolinite crystallinity. *Mineralogical Magazine*, **62A**, 452–454.

Fulignati, P., Malfitano, G., and Sbrana, A. (1997) The Pantelleria caldera geothermal system: Data from the hydrothermal minerals. *Journal of Volcanology and Geothermal Research*, **75**, 251–270.

García Dueñas, V., Balanya, J.C., and Martínez Martínez, J.M. (1992) Miocene extensional detachments in the outcropping basements of the northern Alboran Basin (Betics). *Geomarine Letters*, **12**, 88–95.

Hecht, L., Thuro, K., Plinninger, R., and Cuney, M. (1999) Mineralogical and geochemical characteristics of hydrothermal alteration and episyenitization in the Königshain granites, northern Bohemian Massif, Germany. *Geologische Rundschau*, **88**, 236–252.

Hedenquist, J.W., Arribas, M.A., and Gonzalez-Urien, E. (2000) Exploration for epithermal gold deposits. Pp. 245–277 in: *Gold in 2000* (S.G. Hagemann and P.E. Brown, editors). *Reviews in Economic Geology*, **13**. Society for Economic Geology.

Henley, R.W. and Ellis, A.J. (1983) Geothermal systems, ancient and modern. *Earth Science Reviews*, **19**, 1–50.

Hernández, J., de Larouzière, F.D., Bolze, J., and Bordet, P. (1987) Le magmatisme néogène bético-rifain et couloir de décrochement trans-Alboran. *Bulletin de la Société Géologique de France*, **3**, 257–256.

Hibti, M. and Marignac, C. (2001) The Hajjar deposit of Guemessa (SW Mesta, Morocco): a metamorphosed syn-sedimentary massive sulphide ore body of the Iberian type

https://doi.org/10.1346/CCMN.2009.0570101 Published online by Cambridge University Press

of volcano-sedimentary massive sulphide deposits. Pp. 281–284 in: *Mineral Deposits at the Beginning of the 21st Century* (A. Piestrzyñski *et al*., editors). Balkema, Rotterdam, The Netherlands.

Instituto Geológico y Minero de España (1974) *Mapa Geológico de España*. Escala 1:50,000. Hoja 1046 (24–42): Sorbas. Servicio de publicaciones Ministerio de Industria.

Jiang, W.T., Peacor, D.R., and Buseck, P.R. (1994) Chlorite geothermometry? Contamination and apparent octahedral vacancies. *Clays and Clay Minerals*, **42**, 593–605.

Kranidiotis, P. and MacLean, W.H. (1987) Systematics of chlorite alteration at the Phelps Dodge massive sulphide deposit, Matagami, Quebec. *Economic Geology*, **82**, 1898–1911.

Laird, J. (1988) Chlorites: metamorphic petrology. Pp. 405–447 in: *Hydrous Phyllosilicates Exclusive of Micas* (S.W. Bailey, editor). Reviews in Mineralogy, **19**, Mineralogical Society of America, Washington, D.C., USA.

Lázaro, C., Ruiz Cruz, M.D., and Sanz de Galdeano, C. (2003) Características metamórficas del Triásico Maláguide en las unidades intermedias del sector de Diezma (Sierra Arana, Cordillera Bética). *Boletín de la Sociedad Española de Mineralogía*, 26, 123–136.

Lee, J.H., Peacor, D.R., Lewis, D.D., and Wintsch, R.P. (1986) Evidence for syntectonic crystallization for the mudstone to slate transition at Lehigh Gap, Pennsylvania, USA. *Journal of Structural Geology*, **8**, 767–780.

Leone, G., Reyes, E., Cortecci, G., Pochini, A., and Linares, J. (1983) Genesis of bentonites from Cabo de Gata, Almería, Spain: A stable isotope study. *Clay Minerals*, **18**, 227–238.

López Munguira, A. and Nieto, F. (2000) Transmission electron microscopy study of very low-grade metamorphic rocks in Cambrian sandstones and shales, Ossa-Morena Zone, southwest Spain. *Clays and Clay Minerals*, **48**, 213–223.

López Ruiz, J. and Rodriguez Badiola, E. (1980) La región volcánica del sureste de España. *Estudios Geológicos*, **36**, 5–63.

Maxwell, D.T. and Hower, J. (1967) High grade diagenesis and low-grade metamorphism of illite in the Precambrian belt series. *American Mineralogist*, **52**, 843–857.

McDowell, S.D. and Elders, W.A. (1980) Authigenic layer silicate minerals in borehole Elmore 1, Salton Sea geothermal field, California, USA. *Contributions to Mineralogy and Petrology*, **74**, 293–310.

Merriman, R.J. and Peacor, D.R. (1991) Very low-grade metapelites: mineralogy, microfrabrics and measuring reaction progress. Pp. 10–60 in: *Low-grade Metamorphism* (M. Frey and D. Robinson, editors). Blackwell Science, Oxford, UK.

Moore, D.M. and Reynolds, R.C., Jr. (1997) *X-ray Diffraction and the Identification and Analysis of Clay Minerals*. 2nd edition. Oxford University Press, Oxford, UK.

Morales-Ruano, S. (1994). Mineralogía, geoquímica y metalogenia de los yacimientos hidrotermales del SE de España. PhD thesis, University of Granada, Spain.

Morales-Ruano, S., Carrillo-Rosúa, F.J., Fenoll Hach-Alí, P., de la Fuente Chacón, F., and Contreras López, E. (2000) Epithermal Cu-Au mineralisation in the Palai-Islica deposit, Almería, southeastern Spain, fluid inclusion evidence of mixing of fluids as guide to gold mineralisation. *The Canadian Mineralogist*, **38**, 553–566.

Nieto, F., Ortega-Huertas, M., Peacor, D.R., and Aróstegui, J. (1996) Evolution of illite/smectite from early diagenesis through incipient metamorphism in sediments of the Basque-Cantabrian Basin. *Clays and Clay Minerals*, **44**, 304–323.

Newman, A.C.D. and Brown, G. (1987) The chemical constitutions of clays. Pp. 1–128 in: *Chemistry of Clays and Clay Minerals* (A.C.D. Newman, editor). Monograph **6,** Mineralogical Society**,** London.

Pineda Velasco, A. (1984) Las mineralizaciones metálicas y su contexto geológico en el área volcánica Neógena del Cabo de Gata (Almería, SE de España). *Boletín Geológico Minero*, **95**, 569–592.

Pouchou, J.L and Pichoir, F. (1984) Un nouveau modèle de calcul pour la microanalyse quantitative per spectrométrie de rayons X. *La Recherche Aèrospatiale*, **3**, 167–192.

Reyes, A.G. (1990) Petrology of Philippine geothermal systems and the application of alteration mineralogy to their assessment. *Journal of Volcanology and Geothermal Research*, **43**, 273–309.

Reynolds, R.C. Jr. (1980) Interstratified clay minerals. Pp. 249–303 in: *Crystal Structures of Clay Minerals and their X-ray Identification* (G.W. Brindley and G. Brown, editors). Monograph **5,** Mineralogical Society, London.

Saccocia, P.J. and Gillis, K.M. (1995) Hydrothermal upflow zones in the oceanic crust. *Earth and Planetary Science Letters*, **136**, 1–16.

Saccocia, P.J. and Seyfried, W.E. (1994) The solubility of chlorite solid solutions in 3.2 wt.% NaCl fluids from 300–400ºC, 500 bars. *Geochimica et Cosmochimica Acta*, **58**, 567–585.

Sánchez España, J., Velasco, F., and Yusta, I. (2000) Hydrothermal alteration of felsic volcanic rocks associated with massive sulphide deposition in the northern Iberian Pyrite Belt (SW Spain). *Applied Geochemistry*, **15**, 1265–1290.

Schmidt, D. and Livi, K.J.T. (1999) HRTEM and SAED investigations of polytypism, stacking disorder, crystal growth, and vacancies in chlorites from subgreenschist facies outcrops. *American Mineralogist*, **84**, 160–170.

Shau, Y.H., Peacor, D.R., and Essene, E.J. (1990) Corrensite and mixed-layer chlorite/corrensite in metabasalts from northern Taiwan: TEM/AEM, EMPA, XRD, and optical studies. *Contributions to Mineralogy and Petrology*, **105**, 123–142.

Simmons, S.F., White, N.C., and John, D. (2005) Geological characteristics of epithermal precious and base metal deposits. Pp. 485–522 in: *Economic Geology 100th Anniversary Volume 1905-2005*, (J.W. Hedenquist *et al*., editors). Society of Economic Geologist Inc., Littleton, Colorado, USA.

Turner, S.P., Platt, J.P., George, R.M.M., Kelley, S.P., Pearson, D.G., and Nowell, G.M. (1999) Magmatism associated with orogenic collapse of the Betic-Alboran domain, SE Spain. *Journal of Petrology*, **40**, 1011–1036.

Vidal, O., Parra, T., and Vieillard, P. (2005) Thermodynamic properties of the Tschermak solid solution in Fe-chlorite: Application to natural examples and possible role of oxidation. *American Mineralogist*, **90**, 347–358.

Walshe, J.L. (1986) A six-component chlorite solid solution model and the conditions of chlorite formation in hydrothermal and geothermal systems. *Economic Geology*, **81**, 681–703.

Zaccarini, F., Garuti, G., Rossi, A., Carrillo Rosúa, F.J., Morales Ruano, S., and Fenoll Hach-Alí, P. (2003) Application of chlorite and fluid-inclusion geothermometry to vein and stratiform Fe-Cu-Zn sulphide deposits of the northern appennine ophiolites (Emilia Romagna and Liguria, Italy). *Atti Ticinensi di Scienze della Terra*, **9**, 109–111.

(*Received 17 April 2007; revised 25 October 2008; Ms. 0019; A.E. W.C. Elliott*)